# Fluid Flow and Entropy Generation through a Throttling Valve

BY

**Holayil A. Al-Otaibi**

A Thesis Presented to the

DEANSHIP OF GRADUATE STUDIES

**KING FAHD UNIVERSITY OF PETROLEUM & MINERALS**

DHAHRAN, SAUDI ARABIA

In Partial Fulfillment of the
Requirements for the Degree of

**MASTER OF SCIENCE**

In

**Mechanical Engineering**

**June 2011**

# KING FAHD UNIVERSITY OF PETROLEUM & MINERALS

DHAHRAN 31261, SAUDI ARABIA

## DEANSHIP OF GRADUATE STUDIES

This thesis, written by Mr. Holayil A. Al-Otaibi under the direction of his thesis advisor and approved by his thesis committee, has been presented to and accepted by the Dean of Graduate Studies, in partial fulfillment of the requirements for the degree of **MASTER OF SCIENCE in MECHANICAL ENGINEERING**.

Thesis Committee

Dr. Ahmet Z. Sahin
(Thesis Advisor)

08/6/2011

Dr. Bekir S. Yilbas
(Member)

Dr. Shahzada Z. Shuja
(Member)

Dr. Amro Al-Qutub
(Department Chairman)

١٥/٩/١١

Dr. Salam A. Zummo
(Dean of Graduate Studies)

عمادة الدراسات العليا
DEANSHIP OF GRADUATE STUDIES

**This Thesis is Gratefully**

**Dedicated**

**To**

**My Parents**

**And**

**My Family**

**ACKNOWLEDGEMENT**

All praise belongs to Allah, glorified is He and exalted; Who gave me the opportunity, strength and persistence to work on this project; and Who helped me in the most difficult of times. I am happy to have had an opportunity to glorify His name in the sincerest way through this small accomplishment and pray to Him to accept my efforts.

First, I would like to thank all people who have encouraged and assisted me to do my MSc thesis. In particular I would like to thank my adviser Prof. Ahmet Z. Sahin for his guidance and advice throughout my project. It was a great chance for me to work with Prof. Sahin who has a wide experience in heat and mass transfer problems, and for which I am very grateful.

I also wish to express my thanks to all the lecturers and staff of the Mechanical Engineering School in the King Fahd University of Petroleum and Minerals for their help throughout this MSc program. Special thanks to Dr Bekir Yilbas and Dr Shahzada Shuja, the faculty members of mechanical engineering department, for their assistance and guidance.

I also wish to thank my colleagues at the Saline Water Desalination Research Institute, in particular Dr Osman Hamed and Dr Khalid Bamardouf for their help and support.

Finally, very special thanks go to my parents and my family for their assistance and encouragement.

# Table of Contents

**Page**

# List of Tables

**Tables** **Page**

# List of Figures

**Figures** **Page**

# THESIS ABSTRACT


**Name:** **Holayil A. Al-Otaibi**


**Title:** **Fluid Flow and Entropy Generation through a Throttling Valve**

**Major Field:** **Mechanical Engineering**

**Date of Degree:** **01 June 2011**


A three-dimensional numerical simulation study was conducted to investigate an adiabatic flow behavior and entropy generation through a throttling valve using FLUENT computational fluid dynamics code. A number of numerical trials were carried out to investigate the effect of flow upstream conditions such as temperature, pressure, and velocity as well as the valve position on the fluid dynamic performance of the valve as well as on entropy generation. Two types of fluid were used to perform this study; water and unused engine oil to explore the relationship between viscosity and entropy generation. Other flow characteristics of the fluid flow such as variation of pressure drop, loss and flow coefficients as well as the cavitation index were obtained and compared with the entropy generation which might lead to an in-depth understanding of the flow behavior and irreversibilities inherit in the throttling valve. The total entropy generation rate was predicted using two methods; one by integrating the volumetric entropy generation rate over the volume and the second by using the pressure drop values across the valve. It was observed that the first method was predicting lower values than the second method as a result of the poor mesh at the viscous sublayer near the wall. It was found that the valve position and upstream velocity have the major impact on the pressure drop and entropy

generation while the temperature effect was not significant. The loss coefficient and flow coefficient values were obtained at different valve positions and consequently other results were estimated in terms of pressure drop and entropy generation at different upstream conditions.

# الملخص

هذا البحث عبارة عن دراسة رقمية ذات ثلاثة أبعاد لاكتشاف سلوك سريان الموائع المعزولة حراريا بالإضافة إلى دراسة تولد الانتروبيا خلال محبس خانق و ذلك باستخدام البرنامج المعروف فلونت. تم تنفيذ عدد من الدراسات الرقمية لبحث تأثير الظروف التشغيلية للمائع قبل دخوله على الحبس كالحرارة و الضغط و السرعة بالإضافة إلى وضعية المحبس (زاوية المحبس) على حركة الموائع و تولد الانتروبيا.

تم استخدام نوعين من الموائع في هذه الدراسة وهما الماء و زيت المحرك وذلك لدراسة العلاقة بين اللزوجة و تولد الانتروبيا. الخصائص الأخرى لسريان الموائع كثابت السريان وثابت الفقد في الضغط بالإضافة إلى مؤشر التآكل ألتجويفي جميعها بحثت و قورنت مع تولد الانتروبيا مما قد يؤدي إلى الفهم العميق لسلوك سريان الموائع و تولد الانتروبيا في المحابس الخانقة.

استخدمت طريقتين لحساب تولد الانتروبيا الكلي: الطريقة الأولى بعمل التكامل الرياضي لمعدل تولد الانتروبيا ألحجمي, والثانية عن طريق استخدام قيم الانحدار في الضغط. و قد وجد أن الطريقة الأولى قد أثمرت عن قيم أقل من نظيرتها الثانية وذلك نتيجة لرداءة التقسيم الشبكي في الطبقات اللزجة المتناهية الصغر بالقرب من جدار المحبس. وقد وجد أيضا أن وضعية المحبس (زاوية المحبس) بالإضافة إلى سرعة سريان المائع هما العاملان المؤثران الأهم على انحدار الضغط وتولد الانتروبيا بينما كان تأثير الحرارة اقل أهمية.

من نتائج هذا البحث المهمة كان حساب قيم ثابت السريان و ثابت الفقد في الضغط عند وضعيات مختلفة للمحبس مما أدى إلى استنباط نتائج إضافية للانحدار في الضغط و تولد الانتروبيا عند ظروف تشغيلية أخرى.

# CHAPTER 1

## INTRODUCTION

### 1.1 Background

Valves form an integral part of pipe systems as they enable opening, closing, diverting, mixing or partially obstructing of the flow passage. [Fester, et al. (2009)]. They are usually classified according to their forms, usage, or the source of power. Valves can be classified into motor operated valves (MOVs), air-operated valves, and fluid pressure-operated valves, according to the source of power. Moreover, they can be classified according to their disc forms into gate valves, glove valves, butterfly valves, and ball valves [Kim, 2009].

The frictional losses arising from pipe fittings are often referred to as ‘minor’ losses and are normally neglected when they constitute less than 5% of the total frictional head losses in the straight pipes [Fester, et al. (2007)]. However, the frictional losses are significant in case of throttling processes due to the high pressure drop as a result of high levels of irreversibility. Based on the second law of thermodynamics, no system can have an efficiency of 100 percent. This happens as a result of the fact that part of the energy of the engine or process is deteriorated by other contributors called irreversibilities. These irreversibilites can be found in many forms such as friction, unrestrained expansion, mixing of two gases, heat transfer across a finite temperature difference, electric

resistance, inelastic deformation of solids, and chemical reactions [Cengel, 1994]. Entropy is an abstract property to measure these deteriorations in the levels of energy. If the entropy of a system increases therefore the system loses part of its energy in no useful manner and consequently this leads to less valuable output energy (Exergy). In the last decades scientists and designers paid more attention towards entropy generation studies which become a very powerful indicator for the optimum designs of a number of processes and thermal applications [Ibanez, 2003]. The aim of this study is to explore the relationship between entropy generation and flow behavior at a throttling valve under different operational conditions.

## 1.2 Aims and Objectives

The main objectives of this project are as follows:

1. Modelling the fluid flow through an industrial throttling valve using CFD FLUENT package and predicting the main flow characteristics and their effect on the performance of the valve.
2. Investigate the effect of main design parameters and configuration of the valve on its performance.
3. Study the entropy generation throughout the valve.
4. Examine available fluid flow models and suitable solution techniques in FLUENT CFD code to perform this kind of study as well as to examine the validity of results.

## 1.3 Motivation

Valves are extensively used in many industrial and nonindustrial fields. From the designers' point of view, the valve design must impose minimum flow resistance and form an effective seal at the proper time. In addition, suitable geometric flow areas, small clearance volumes, simple and rugged design should be combined [Arztmann (2002)]. On the other hand, for optimum design of a control valve driving system, a preliminary estimation of the driving forces is needed. This can be carried out by experimental measurements or numerical analysis which can be performed by means of either Computational Fluid Dynamics (CFD) codes or theoretical models based on the momentum conservation law [Amirante et al. (2006)].

The selection of inefficient and oversized pumps is a common result of conservative estimates for the loss of pipe fitting such as valves [Fester et al. (2007)]. Throttling valves are responsible for a significant portion of energy loss in a number of applications. In some applications the throttling process is conducted by means of turbine engines to utilize the reduction of pressure in generating power or driving another part of the process. However, this integration is not always applicable especially if a number of systems utilize a common source of energy such as high pressure steam generator.

The relationship between irreversibility and flow behavior at a throttling valve was investigated in this study. Three upstream conditions of temperature, pressure, and velocity as well as the valve position were considered in this investigation. The impact of upstream temperature was examined for two types of fluids which are water and unused engine oil.

The selection of fluids is based on the current wide usage of these fluids in the petrochemical industry.

Generally, valves studies are very important for a broad range of groups such as valves manufacturers, designers of industrial processes, technical people of large power plants and factories, energy reducing claimants, and scientists. From the literature review it was found that the previous studies on valves are mainly focusing on the dynamic characteristics of fluid flow such as the variation of pressure drop, loss coefficient and flow coefficient as well as the cavitation index for different upstream conditions. On the other hand the previous entropy generation studies were focusing on the heat exchanging processes and thermal applications. In this study the novelty might be in modeling the fluid flow and entropy generation in a throttling valve. The impact of entropy generation on fluid flow characteristics was carried out under different operating conditions which might provide a better understanding about throttling processes.

# CHAPTER 2

# LITERATURE REVIEW

## 2.1 Entropy Generation

The irreversibility in non reacting processes is associated to two forms of losses; the viscous irreversibility, and the heat transfer irreversibility. In this part, the entropy generation is reviewed for both mentioned forms in order to provide a clear picture on irreversibility and its forms.

A good reference for the general procedure for entropy generation minimization (EGM) was introduced by Bejan (1996). In this method the heat transfer, fluid flow, and mass transfer irreversibilities are combined at the most fundamental levels to predict the thermodynamic optimization of a system. For more information, it can also be refer to Bejan (1982, 1988, and 1996). The geometries of flow passage play a significant role in entropy generation for both forms of irreversibility. The combination impact of geometry on both forms of irreversibility was examined by a number of investigators. Bejan (1979) has applied this analysis on the forced convective heat transfer for different configurations (pipe, flat plate, single cylinder in cross flow, and flow in the entrance of rectangular duct) and studied the affect of their geometry on the irreversibilities through the relationship between the duty parameter and the Reynolds number. He found that as the aggregate duty

parameter increases, the optimum tube radius decreases (Re increases) and minimum entropy generation also decreases.

Sahin [1998(a)] studied a second law comparison for optimum shape of duct. His study included several cross sectional duct geometries to investigate their effect on entropy generation as well as on pumping power. He found that the optimum duct geometry for constant thermo-physical properties depends on the Reynolds number. Moreover, the circular geometry is the optimum one especially when the viscous dissipation is the dominant and the triangular and rectangular geometries are the worst in terms of irreversibility and pumping power.

A study of the effect of cross sectional area, heat flux, and Reynolds Number on the entropy generation in semi-cylindrical duct was also carried out by Oztop (2005). He found that as the cross sectional area and heat flux increase, both entropy generation and pumping power ratio increase at a fixed Reynolds number. Ko and Ting (2006) have also conducted a study to examine the forced convection in a curved rectangular duct with external heating. The effects of Dean Number, external wall heat flux, and cross-sectional aspect ratio were investigated. They found that the area exposed to heat transfer was having high heat transfer entropy generation comparing to the viscous entropy generation while it was vice versa for the area which was an adiabatic. The competition between viscous irreversibility and heat transfer irreversibility was complex relating to Reynolds number, heat flux and aspect ratio. This was making the relationship between total entropy generation and heat flux non monotonous.

Ko (2006) also investigated similar study for the entropy generation in a double-sine duct which is frequently used in plate heat exchangers. In his study, he included the effect of The Reynolds number, wall heat flux, and the aspect ratio on the entropy generation. The results show that viscous irreversibility will become more dominated in cases with larger Reynolds number and smaller heat flux, while heat transfer irreversibility will become more dominated in cases with smaller Reynolds number and larger heat flux.

On the other hand, various studies were conducted to investigate the effect of heat transfer enhancement on entropy generation. Dagtekin, et al. (2005) studied the entropy generation analysis in a circular duct with internal longitudinal fins. Three different fin shapes are chosen for the analysis: Thin, triangular and V-shaped fins. It was found that the number of fins and dimensionless length of the fins have significant effect on both entropy generation and pumping power. As the Reynolds number is increased, the entropy generation decreases and the pumping power to heat transfer ratio increases in all the cases considered. However, as the inlet to wall temperature difference increases, the entropy generation increases and the pumping power to heat transfer ratio decreases in all the cases considered. They also found that as the number of thin or triangular fins is increased, the dimensionless entropy generation increases. In addition, as the length of the fins is increased, the dimensionless entropy generation and the pumping power to heat transfer ratio increase and they depend on dimensionless fin length values.

Eiamsa-ard (2010) studied the influences of multiple twisted tape vortex generators on the heat transfer and fluid friction characteristics in a rectangular channel. The influences of

free spacing ratio, twist ratio and Reynolds number on the heat transfer rate, flow friction and enhancement index behaviors are investigated. It was found that the decreases of both free-spacing ratio and twist ratio resulted in the increases of Nusselt number, friction factor and also enhancement index. The Nusselt numbers increase in the range of 10% and 170% in comparison with the values in the smooth channel while the friction factors are in the range of 1.45 and 5.7 times of those for the smooth channel.

Isaev, et al. (2010) have conducted a study to investigate the Influence of the Reynolds number and the spherical dimple depth on turbulent heat transfer and hydraulic loss in a narrow channel. It was found that the depth to diameter ratio and the Reynolds number have a significant effect on the flow and heat transfer as well as on entropy production. Their study was examined the heat transfer and pressure loss under spherical small-depth (0.13) and large-depth (0.26) dimples and Reynolds number ranges from $2x10^4$ to $6x10^4$. Air was chosen as fluid, and the long channel walls have a temperature of 373 K (with a dimple) and 293 K and the side walls are adiabatic. It was observed that increasing the Reynolds number yielding local changes in the flow structure and in the zones of elevated and reduced relative heat fluxes however no remarkable effect on integral relative heat transfer. Simultaneously, the hydraulic loss grows essentially as Reynolds number is increased.

Other analytical studies have focused on the effect of the entropy generation and boundary conditions on flow characteristics and pumping power. The entropy generation in a duct is a result of both the heat transfer and viscous friction. Sahin [1998(b)] has carried out a

study for laminar flow through a duct subjected to constant wall temperature. He studied a constant viscosity case along with two cases for viscosity temperature dependant for water and glycerol. The optimum pipe length and optimum inlet temperature at constant wall temperature were investigated based on the principle of entropy generation minimization. Sahin [2000] has carried out a similar study on the entropy generation and pumping power in a turbulent fluid flow through a smooth pipe subjected to constant heat flux. He reported that the temperature dependence of the viscosity and consequently the viscosity variation has a considerable effect on both the entropy generation and the pumping power. It was found that pumping power to heat transfer ratio and the entropy generation per unit heat transfer can become very large especially for low heat flux conditions.

The effect of fouling formation on the thermodynamic performance was reported in a number of studies. Sahin, et al., (2000) have examined the effect of fouling formation on entropy production and pressure losses. The effect of fouling with entropy generation and related operational cost was investigated. The fouling thickness and tube surface temperature are considered to be the main parameters. It was observed that fouling has a considerable effect on the irreversibility components due to heat transfer and pressure drop in viscous pipe flow. The irreversibility due to viscous friction increases faster than that due to heat transfer. Wu, et al., (2007) have similar study evaluating the effect of fouling on the thermodynamic performance of forced convective heat transfer through a duct. The effects of Reynolds number, thickness of fouling layer, dimensionless inlet temperature difference and wall heat flux on the exergy variation of working fluids was investigated. It was found that the exergy variation degradation rate increases with the increase of

Reynolds number and decreases with the increase of dimensionless inlet temperature and wall heat flux. The results show also that the effect of fouling on the exergy variation of working fluids in convective heat transfer processes with constant wall temperature is relatively different from that with constant wall heat flux in some ways when fouling appears and the mass flow rate of the fluid is kept constant. Besides, the exergy variation caused by heat conduction of the fouling plays an important role in the total exergy variation of working fluids.

## 2.2 Flow Characteristics at Throttling Devices

Several studies have been carried out to investigate the flow patterns and fluid dynamics in different types of throttling devices. The expanding and contraction of the flow passage has a significant effect on entropy generation. Yapıcı, et al., (2005) studied the local entropy generation in compressible flow through a suddenly expanding pipe. Their study investigates the effect of expansion ratio, the mass flux, the ambient heat transfer coefficient, and the inlet temperature on the entropy generation. A 2-D simulation was performed by using FLUENT computational fluid dynamics (CFD) code and another computer program written in FORTRAN 77 language. It has been developed to calculate numerically the volumetric entropy generation rate distributions and the other thermodynamic parameters by using the results of the calculations performed with the FLUENT program. It was found that the contraction of the radius of the throat increases significantly the maximum value of the volumetric entropy generation rate (about 60%) and raises exponentially 11 times the total entropy generation rate with respect to the its

base value. The normalized merit number (the ratio of exergy transferred to the sum of exergy transferred and exergy destroyed) decreases with the contraction of the cross-section and with the increase of the ambient heat transfer coefficient, while it rises with the decrease of the maximum mass flux and with the increase of the inlet temperature.

Biyikoglu (2009) has studied the entropy generation due to flow across a contraction of pipe joint. The simulation of flow and entropy generation rate due to viscous dissipation was carried out for different upstream Reynolds numbers. It was noticed that entropy generation rate increases with increasing Reynolds number due to the high rate of fluid strain immediately after the contraction plane. Although the location of maximum entropy generation rate in the radial direction remains approximately the same for different Reynolds numbers, however, the axial location of maximum entropy generation rate changes with changing Reynolds numbers. It was also found that overshooting of axial velocity occurs in the vicinity of the plane of contraction is responsible for the high entropy generation rate after the contraction plane.

Iandoli and Sciubba (2005) have studied the entropy generation through a radial compressor stage. Their study was conducted using LES turbulent model by means of Fluent CFD program. Both radial and tangential secondary flows were identified in the rotor and in the diffuser. The results of entropy generation were used to identify a number of issues such as the sonic effects in the throat region which have an effect on the pressure recovery by introducing a local expansion as well as the counter flow by the effect of adverse pressure gradient.

Pereira and Ramos (2010) have studied the flow characteristics such as flow coefficient, cavitation index, and loss coefficient through different types of valves. The effect of the angle of a ball valve as well as the pressure and velocity were obtained. It was also found that the size of the ball valve has significant influence on these characteristics. M. Chern, et al. (2007) investigated the flow patterns across a ball valve. Various patterns of flows upstream and downstream the ball valves with respect to different valve openings and inlet velocities are visualized using a particle tracking flow visualization method (PTFV). The valve performance was determined by calculating the loss coefficient and flow coefficient as well as cavitation index using the pressure and flow rate data.

Song, et al. (2009) studied a fluid analysis and a topology optimization for a butterfly valve. The fluid field analysis was conducted to observe the flow patterns and to evaluate the flow characteristics of valve when the valve disc is opened $15^{o}$. A steady simulation was performed assuming, uniform temperature through the fluid flow with water at a temperature of 25 $^{o}$C. Based on the CFD fluid flow analysis, the pressure loss coefficient was calculated and a topology optimization using finite element method for a STS316 valve disk was made.

Rahaman, et al. (2007) have developed a CFD model to investigate the complex flows in a product fill valve that is used for packaging liquid products. A numerical simulation for pressure, velocity and wall shear stress distribution was conducted and consequently some modifications have been suggested to avoid the reverse flow at the outlet of the valve and cavitation at other regions. Henderson, et al. (2007) have conducted a study to explore the

flow through a safety butterfly valve used in a hydro-electric power scheme to stop water supply to a downstream penstock. Their study has focused on the hydrodynamic torque versus opening angle characteristics during a constant head test. The effect of Reynolds number and unsteady flow was found considerable.

Eiamsa-ard, et al., (2008) have carried out a research study on the flow through circular orifice using computational fluid dynamics (CFD) with different turbulence models. Their study focused on the effect of orifice diameter ratios (d/D) on flow field characteristics. A comparison between the standard k-E model and Reynolds Stresses model was considered. It was found that the RSM model has leaded to a good agreement with the experimental results.

Parlak, et al., (2011) have studied a second law analysis for a steady-laminar flow of water in adiabatic microtubes. Smooth microtubes made of fused silica with diameters between 50 and 150 micrometer were used in their experiments. It was observed a significant temperature rises due to viscous dissipation and relatively high pressure losses of flow. The rate of entropy generation from the experiments has been determined in a flow of Reynolds number ranges from 20 to 2200. The second law analysis results showed that the flow characteristics in the smooth microtubes are distinguished considerably from the conventional theory for flow in the larger tubes with respect to viscous heating, total entropy generation rate, and exergy losses.

# CHAPTER 3

# PROBLEM FORMULATION

## 3.1 Statement of the Problem

A three-dimensional numerical simulation study was conducted to investigate an adiabatic flow behavior and fluid dynamics as well as to carry out the calculation of entropy generation across a Full-Port ball valve, see figure 1. This was carried out using FLUENT computational fluid dynamics code. At first, the study was commence by drawing the domain of the study in Gambit software (ANSYS Package) and finding out the suitable mesh which leaded to less numerical diffusion and skewness problems. Then it was exported to the FLUENT software where other solution techniques and setting of boundary conditions are needed. The custom field function provided in the software was used to conduct the computation of local entropy generation throughout the valve.

Figure 1: A schematic diagram for a ball valve

This study was focused on the impact of five variables on the behavior of fluid flow inside the throttling valve as can be seen from figure 2. These variables as also shown also in table 1 are upstream velocity, upstream pressure, upstream temperature, angle of valve, and two types of fluids.

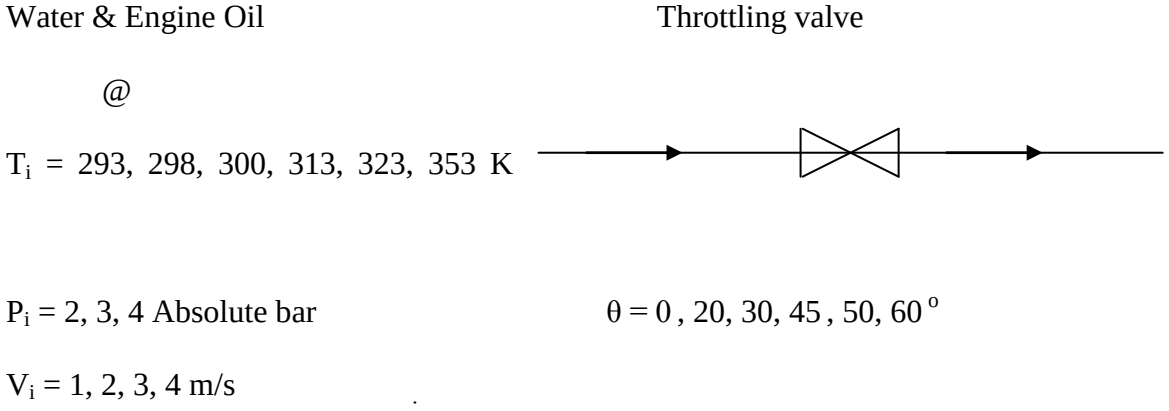


Figure 2: Upstream conditions and valve positions of the current study

**Table 1: Upstream Conditions**

| Variable | Unit | Values considered | | | | | |
|---|---|---|---|---|---|---|---|
| Temperature, $T_i$ | K | 293 | 298 | 300 | 313 | 323 | 353 |
| Angle of Valve, θ | degree | 0 | 20 | 30 | 45 | 50 | 60 |
| Velocity, $V_i$ | m/s | 1 | 2 | 3 | 4 | - | - |
| Pressure, $P_i$ | bar | 2 | 3 | 4 | - | - | - |
| Fluids | - | Water | Engine Oil | - | - | - | - |

The details of all cases will be illustrated in chapter 5.

## 3.2 Flow Motion Governing Equations

The well-known Navier-Stokes equations of motion for general linear (Newtonian) compressible, viscous fluid and neglected body forces can be written in the following forms:

**Continuity**

$$\frac{\partial \rho}{\partial t} + \frac{\partial}{\partial x_j}\left(\rho u_j\right) = 0 \tag{3.2.1}$$

**Momentum**

$$\frac{\partial}{\partial t}\left(\rho u_i\right) + \frac{\partial}{\partial x_j}\left(\rho u_i u_j\right) = -\frac{\partial P}{\partial x_i} + \frac{\partial \tau_{ij}}{\partial x_j} \tag{3.2.2}$$

**Energy**

$$\frac{\partial}{\partial t}\left(\rho H\right) + \frac{\partial}{\partial x_j}\left(\rho u_j H\right) = \frac{\partial P}{\partial t} + \frac{\partial}{\partial x_j}\left(u_i \tau_j - q_j\right) \tag{3.2.3}$$

Where the stress tensor $\tau_{ij}$, heat-flux vector $q_j$, and total enthalpy $H$ are given by

$$\tau_{ij} = \lambda \delta_{ij} \frac{\partial u_l}{\partial x_l} + \mu \left(\frac{\partial u_i}{\partial x_j} + \frac{\partial u_j}{\partial x_i}\right) \tag{3.2.4}$$

$$q_j = -\kappa \frac{\partial T}{\partial x_j} \tag{3.2.5}$$

$$H = h + \frac{1}{2} u_i u_j \tag{3.2.6}$$

In these equations, $\lambda$ is the bulk viscosity (=-2/3$\mu$), $\mu$ the dynamic viscosity, $\kappa$ the thermal conductivity, and $h$ the static enthalpy. In Eq.3.2.4, $\delta_{ij}$ is the Kronecker delta, have the value 1 for $i=j$ and 0 for $i \neq j$. A summation is understood for repeated indices.

These equations are valid for both laminar and turbulent flows, however the actual computation of a raw velocity component *u(x,y,z,t)* is not possible for the turbulent flows. Therefore the standard method is to separate the fluctuating properties from their time-mean values. For turbulent flow, the velocity components, pressure, and temperature can be expressed as sums of their mean values and fluctuations.

$$u = \bar{u}(x,y,z,t) + u'(x,y,z,t)$$
$$v = \bar{v}(x,y,z,t) + v'(x,y,z,t)$$
$$w = \bar{w}(x,y,z,t) + w'(x,y,z,t)$$
$$p = \bar{p}(x,y,z,t) + p'(x,y,z,t)$$
$$T = \bar{T}(x,y,z,t) + T'(x,y,z,t)$$

The general forms of turbulent flow equations are as follows:

**Continuity**

$$\frac{\partial}{\partial t} + \frac{\partial}{\partial x_j}\left(\bar{\rho}\,\bar{u}_j\right) = 0 \qquad (3.2.7)$$

**Momentum**

$$\frac{\partial}{\partial t}\left(\bar{\rho}\,\bar{u}_i\right) + \frac{\partial}{\partial x_j}\left(\bar{\rho}\,\bar{u}_i\bar{u}_j\right) = -\frac{\partial P}{\partial x_i} + \frac{\partial}{\partial x_j}\left(\tau_{ij} - \overline{\rho u_i' u_j'}\right) \qquad (3.2.8)$$

**Energy**

$$= \frac{\partial \bar{P}}{\partial t} + \frac{\partial}{\partial x_j}\left(-\bar{q}_j - \overline{\rho \acute{H} \acute{u}_j} + \bar{u}_j \bar{\tau}_{ij} + \overline{\acute{u}_j \tau_{ij}}\right) \quad (3.2.9)$$

For incompressible turbulent flow, they can be expressed in more details as following:

**Continuity**

$$\frac{\partial \bar{u}}{\partial x} + \frac{\partial \bar{v}}{\partial y} + \frac{\partial \bar{w}}{\partial z} = 0 \quad (3.2.10)$$

**Momentum in X-direction**

$$\frac{\partial \bar{u}}{\partial t} + \bar{u}\frac{\partial \bar{u}}{\partial x} + \bar{v}\frac{\partial \bar{u}}{\partial y} + \bar{w}\frac{\partial \bar{u}}{\partial z} \quad (3.2.11)$$

$$= -\frac{1}{\rho}\frac{\partial \bar{p}}{\partial x} + \vartheta\left(\frac{\partial^2 \bar{u}}{\partial x^2} + \frac{\partial^2 \bar{u}}{\partial y^2} + \frac{\partial^2 \bar{u}}{\partial z^2}\right) - \left(\frac{\partial \overline{\acute{u}^2}}{\partial x} + \frac{\partial \overline{\acute{v}\acute{u}}}{\partial y} + \frac{\partial \overline{\acute{w}\acute{u}}}{\partial z}\right)$$

**Momentum in Y-direction**

$$\frac{\partial \bar{v}}{\partial t} + \bar{u}\frac{\partial \bar{v}}{\partial x} + \bar{v}\frac{\partial \bar{v}}{\partial y} + \bar{w}\frac{\partial \bar{v}}{\partial z} \quad (3.2.12)$$

$$= -\frac{1}{\rho}\frac{\partial \bar{p}}{\partial y} + \vartheta\left(\frac{\partial^2 \bar{v}}{\partial x^2} + \frac{\partial^2 \bar{v}}{\partial y^2} + \frac{\partial^2 \bar{v}}{\partial z^2}\right) - \left(\frac{\partial \overline{\acute{v}\acute{u}}}{\partial y} + \frac{\partial \overline{\acute{v}^2}}{\partial x} + \frac{\partial \overline{\acute{w}\acute{v}}}{\partial z}\right)$$

**Momentum in Z-direction**

$$\frac{\partial \bar{w}}{\partial t} + \bar{u}\frac{\partial \bar{w}}{\partial x} + \bar{v}\frac{\partial \bar{w}}{\partial y} + \bar{w}\frac{\partial \bar{w}}{\partial z} \tag{3.2.13}$$

$$= -\frac{1}{\rho}\frac{\partial \bar{p}}{\partial x} + \vartheta\left(\frac{\partial^2 \bar{w}}{\partial x^2} + \frac{\partial^2 \overline{v}\overline{w}}{\partial y^2} + \frac{\partial^2 \bar{w}}{\partial z^2}\right) - \left(\frac{\partial \overline{u'w'}}{\partial x} + \frac{\partial \overline{v'w'}}{\partial y} + \frac{\partial \overline{\acute{w}^2}}{\partial z}\right)$$

Where $\vartheta$ is the kinematic viscosity

**Energy**

$$\frac{\partial \overline{\mathrm{T}}}{\partial t} + \bar{u}\frac{\partial \overline{\mathrm{T}}}{\partial x} + \bar{v}\frac{\partial \overline{\mathrm{T}}}{\partial y} + \bar{w}\frac{\partial \overline{\mathrm{T}}}{\partial z} \tag{3.2.14}$$

$$= \alpha\left(\frac{\partial^2 \overline{\mathrm{T}}}{\partial x^2} + \frac{\partial^2 \overline{\mathrm{T}}}{\partial y^2} + \frac{\partial^2 \overline{\mathrm{T}}}{\partial z^2}\right) - \left(\frac{\partial \overline{u'\mathrm{T}'}}{\partial x} + \frac{\partial \overline{v'\mathrm{T}'}}{\partial y} + \frac{\partial \overline{w'\mathrm{T}'}}{\partial z}\right)$$

Where $\alpha$ is the thermal diffusivity

To express the partial derivatives of the time-averaged values of fluctuations in terms of mean values, scientists attempt has been carried out to find the most widely additional relations which are the turbulence kinetic energy and Reynolds stress equations.

**Turbulence kinetic energy**

$$K = \frac{1}{2}\left(\overline{u'^2} + \overline{v'^2} + \overline{w'^2}\right) \tag{3.2.15}$$

The conservation relation for $K$ is as follows:

$$\frac{D}{Dt}\left(\bar{\rho}\frac{\tilde{u}_i\tilde{u}_i}{2}\right) = -\tilde{u}_i\frac{\partial \bar{p}}{\partial x_i} + \tilde{u}_i\frac{\partial \bar{\tau}_{ik}}{\partial x_k} - \tilde{u}_i\frac{\partial}{\partial x_k}\left(\rho u_i' u_k'\right) \tag{3.2.16}$$

Where:

$$\frac{D}{Dt}\left(\bar{\rho}\frac{\tilde{u}_i\tilde{u}_i}{2}\right) = \frac{\partial}{\partial t}\left(\bar{\rho}\frac{\tilde{u}_i\tilde{u}_i}{2}\right) + \frac{\partial}{\partial x_k}\left[\tilde{u}_k\left(\bar{\rho}\frac{\tilde{u}_i\tilde{u}_i}{2}\right)\right] \tag{3.2.17}$$

And

$$-u_i\frac{\partial}{\partial x_k}\overline{\rho u_i' u_k'} = -\frac{\partial}{\partial x_k}\left(u_i\overline{\rho u_i' u_k'}\right) + \overline{\rho u_i' u_k'}\frac{\partial u_i}{\partial x_k} \tag{3.2.18}$$

**Reynolds Stress Equation**

Referring to equation (3.2.8), we can notice the last term which is called turbulent or Reynolds stress:

$$\sigma_{ij} = -\rho\overline{u_i u_j} \tag{3.2.19}$$

The transport equation of Reynolds stress term can be written as follows:

$$\begin{aligned}&\frac{D}{Dt}\left(\overline{\rho u_i' u_j'}\right) + \frac{\partial}{\partial x_k}\left(\overline{\rho u_i' u_j' u_k'}\right)\\ &= -\overline{u_j'\frac{\partial p}{\partial x_i}} - \overline{u_i'\frac{\partial p}{\partial x_j}} + \overline{u_j'\frac{\partial \tau_{ik}''}{\partial x_k}} + \overline{u_i'\frac{\partial \tau_{jk}''}{\partial x_k}}\\ &-\rho u_i' u_k'\frac{\partial \bar{u}_j}{\partial x_k} - \overline{\rho u_j' u_k'}\frac{\partial \bar{u}_i}{\partial x_k}\end{aligned} \tag{3.2.20}$$

and

$$\frac{D}{Dt}\left(\overline{\rho u_i' u_j'}\right) = \frac{\partial}{\partial t}\left(\overline{\rho u_i' u_j'}\right) + \frac{\partial}{\partial x_k}\left(\tilde{u}_k\overline{\rho u_i' u_j'}\right) \tag{3.2.21}$$

### 3.3 Modelling of Turbulent Flow

Modeling of turbulent flow has become a mature science. There are plenty of publications which can describe important issues related to this field. The complexity range of modeling turbulent flow can be seen in figure 3.

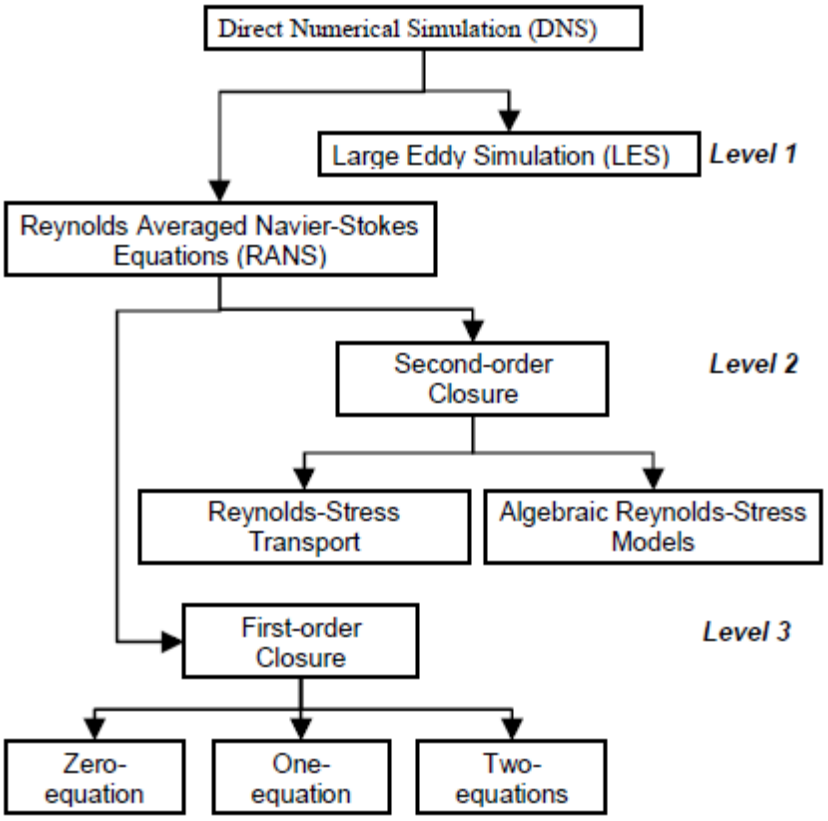


Figure 3: Levels for turbulence modeling (Uygun, et al 2004)

A brief explanation for these levels is illustrated below (White 2006, Uygun et al 2004):

- Direct Numerical Simulation (DNS): Compute full Navier-Stokes equations without averaging and all time and length scales are resolved; however it is limited to low-turbulent Reynolds numbers with simple geometrical domain.
- Large-eddy Simulation (LES): Compute full Navier-Stokes equations without averaging for motion scales of order equal or larger than the grid size and use turbulence models for small scales. It is limited to moderate Reynolds numbers.
- Second-Closure Model: the most complex time-averaging turbulent model. Compute the dissipation equation, ignores the turbulent kinetic energy and model the full Reynolds stress equation.
- Two-equation Model: adds the turbulent kinetic energy and a second partial differential equation which is usually dissipation rate equation as well as additional algebraic formulas.
- One-equation Model: adds either turbulence kinetic energy or eddy viscosity equation in addition to algebraic formulas.
- Zero-equation Model: adds algebraic eddy-viscosity formulas.

In this study, four turbulent models are used:

- Two-equation Models:
  - Standard k-ε
  - RNG k-ε model
  - Realizable k-ε mode
- Reynolds Stress Model

More details about them are given in Chapter4.

### 3.4 Entropy Generation

The entropy generation in most thermal fluid systems is usually a result of two processes; heat transfer and viscous dissipation. This can be seen clearly from the relation between entropy and both pressure and temperature which can be expressed as following:

$$ds = \frac{dh}{T} - \frac{v}{T} dP \tag{3.4.1}$$

Where $h$ is the specific enthalpy and $v$ is the specific volume

From second law of the thermodynamics the entropy conservation equation for a control volume can be written as:

$$\dot{S}_{gen} = \frac{\partial s}{\partial t} - \frac{\dot{Q}}{T_o} - \sum_{in} \dot{m}s + \sum_{out} \dot{m}s \tag{3.4.2}$$

Where:

$\dot{Q}$ : heat transfer rate

$\dot{m}$ : mass flow rate

s : specific entropy

$T_o$ : boundary temperature of the system

In vectorial notation the volumetric entropy generation rate can be expressed as follows:

$$\dot{S}'''_{gen} = \frac{1}{T} q.\nabla T - \frac{1}{T^2} q.\nabla T + \rho \frac{DS}{Dt} \tag{3.4.3}$$

$$ds = \frac{du}{T} - \frac{P}{T} dv \tag{3.4.4}$$

Considering the substantial derivative of equation (3.4.4):

$$\rho \frac{Ds}{Dt} = \frac{\rho}{T} \frac{Du}{Dt} - \frac{P}{\rho T} \frac{D\rho}{Dt} \tag{3.4.5}$$

From first law of thermodynamics energy equation can be expressed as:

$$\rho \frac{Du}{Dt} = -\nabla . q - p\,(\nabla . V) + \mu\,\Phi \tag{3.4.6}$$

Where Φ is the viscous dissipation

By substitute equation (3.4.6) into equation (3.4.5) and combining with equation (3.4.3) it gives:

$$\dot{S}'''_{gen} = -\frac{1}{T^2} q . \nabla T + \frac{\mu}{T} \Phi \tag{3.4.7}$$

It can be further simplified by using Fourier's heat conduction law

$$q = -k \nabla T \tag{3.4.8}$$

By substituting the above equation in the entropy equation, the final volumetric entropy generation equation can be written as:

$$\dot{S}_{gen}^{'''} = \frac{k}{T^2}\,(\nabla T)^2 + \frac{\mu}{T}\Phi \tag{3.4.9}$$

In more detailed form, it can be written as following:

$$\dot{S}_{v}^{'''} = \frac{\mu}{T}\left\{\begin{array}{c} 2\left[\left(\frac{\partial u}{\partial x}\right)^2 + \left(\frac{\partial v}{\partial y}\right)^2 + \left(\frac{\partial w}{\partial z}\right)^2\right] \\ + \left(\frac{\partial u}{\partial z} + \frac{\partial w}{\partial x}\right)^2 + \left(\frac{\partial u}{\partial y} + \frac{\partial v}{\partial x}\right)^2 \\ + \left(\frac{\partial v}{\partial z} + \frac{\partial w}{\partial y}\right)^2 \end{array}\right\} \tag{3.4.10}$$

$$\dot{S}_{t}^{'''} = \frac{k}{T^2}\left[\left(\frac{\partial T}{\partial x}\right)^2 + \left(\frac{\partial T}{\partial y}\right)^2 + \left(\frac{\partial T}{\partial z}\right)^2\right] \tag{3.4.11}$$

Where $\dot{S}_{v}^{'''}$ is the volumetric entropy generation rate due to the viscous dissipation and $\dot{S}_{t}^{'''}$ is the volumetric entropy generation rate due to heat transfer. However, in this study the system is assumed to be an adiabatic and the internal heat transfer is negligible due to the small change in temperature; therefore only the viscous part of the above equations will be considered. For turbulent flow, the viscosity and thermal conductivity in the above equations should be replaced by *effective viscosity* and *effective thermal conductivity* which can be obtained from the turbulent model as reported by Makhanlall, et al. (2010).

Two methods were used to calculate the total entropy generation throughout the valve in this study.

**First method**: by integration of the volumetric local entropy generation rate (W/K.m$^3$) over the volume, equation (3.4.7):

$$\dot{S}_g = \int \dot{S}_g''' \, dV \quad = \int (-\frac{1}{T^2} q.\nabla T + \frac{\mu}{T}\Phi) \, dV \tag{3.4.11}$$

The viscous part is only considered because the problem is an adiabatic and the difference in temperature is very small.

**Second method**: by using the general equation of entropy change (J/kg.K) which is function of change of enthalpy and pressure (3.4.1) and multiply it by the mass flow rate. The change of enthalpy is neglected because it is throttling process.

$$\dot{S}_g = \dot{m} * \, ds = \dot{m} * ( \, \frac{dh}{T} - \frac{v}{T} dP) \tag{3.4.11}$$

## 3.5 Flow Characteristics through a Throttling Valve

There are three important coefficients used to evaluate the performance of valves; the loss coefficient, the flow coefficient and the cavitation index (M. Chern and C. Wang, 2004).

**The loss coefficient**

It is defined as the ratio of pressure drop to the inlet kinetic Energy as can be seen from equation (3.5.1)

$$K \; = \; \frac{\Delta P}{\frac{1}{2}\rho \, U_i^2} \tag{3.5.1}$$

Where $U_i$ (m/s) is the mean inlet velocity, $\Delta P$ (Pascal) is the pressure drop measured between 2D in front of the valve and 6D behind the valve.

**The flow coefficient**

It is the ratio of volumetric flow rate to the pressure drop:

$$C_v = \frac{q}{0.0865\,F_p}\sqrt{\frac{G}{\Delta P}} \tag{3.5.2}$$

Where $q$ is the volume flow rate ($m^3/h$), $\Delta P$ is the pressure drop (KPa), $G$ is the specific gravity relative to water at 4°C and $F_p$ is the geometric factor which equals one in this case.

**The cavitation index**

It can be defined as the ratio of pressure drop across the valve to the range of pressure between the inlet pressure and the vapour pressure.

$$C_{cs} = \frac{\Delta P}{P_{in} - P_v} \tag{3.5.3}$$

Where $P_v$ refers to the saturated vapor pressure.

# CHAPTER 4

# NUMERICAL APPROACH

One of the main objectives of this thesis is to understand how to set up and solve the numerical simulation problems and to be familiar with FLUENT, CFD software. In this chapter, a general idea is given about the CFD and then followed by a number of significant points of how the solution was established.

## 4.1 CFD (Computational Fluid Dynamics)

In CFD (Computational Fluid Dynamics) the mass and heat transfer problems and other related problems such as chemical reactions can be solved numerically. Each CFD code has to operate following three steps: Pre-processing, Solving, and Post-processing.

**Pre-processing**

It requires a number of settings such as definition of the domain, generation of geometry and grid, setting of the boundary conditions, and identifying fluid properties.

**Solving**

CFD can be used in three discretization methods: Finite difference method (FDM), Finite element method (FEM), or Finite volume method (FVM) which is implemented in FLUENT code, the code of this study. The finite volume method (FVM) is designed

to transfer continuous models and equations into distinguished finite volume or cell. A variety of finite-difference-type approximations for the terms in the integrated equation are applied in order to convert the integral equations into algebraic equations (Versteeg, 1995).

**Post-processing**

It provides a variety of results such as, grid display, domain geometry, vector plots, particle tracking, and a number of visual results.

## 4.2 Meshing of the Model

For every numerical simulation, the domain and number of cells plays a significant role in the accuracy of the solution. The pre-processer GAMBIT, which is developed by ANSYS, is used to generate and mesh the domain. GAMBIT is considered to be one of the advanced pre-processors, which can generate and mesh the domain in a powerful and flexible way.

**Pipe length**

The pipe length before the valve was set to 2D (two times the diameter of the valve) and 6D (six times the diameter of the valve) after the valve based on initial trials to discover the effect of presence of the valve on the velocity profile.

**Mesh Generation**

In this study, the mesh generation have been carried out in two steps. The first step was generating the mesh in GAMBIT with HEX/WEDGE scheme and an interval size of 0.004 as shown in the figures 4 and 5.

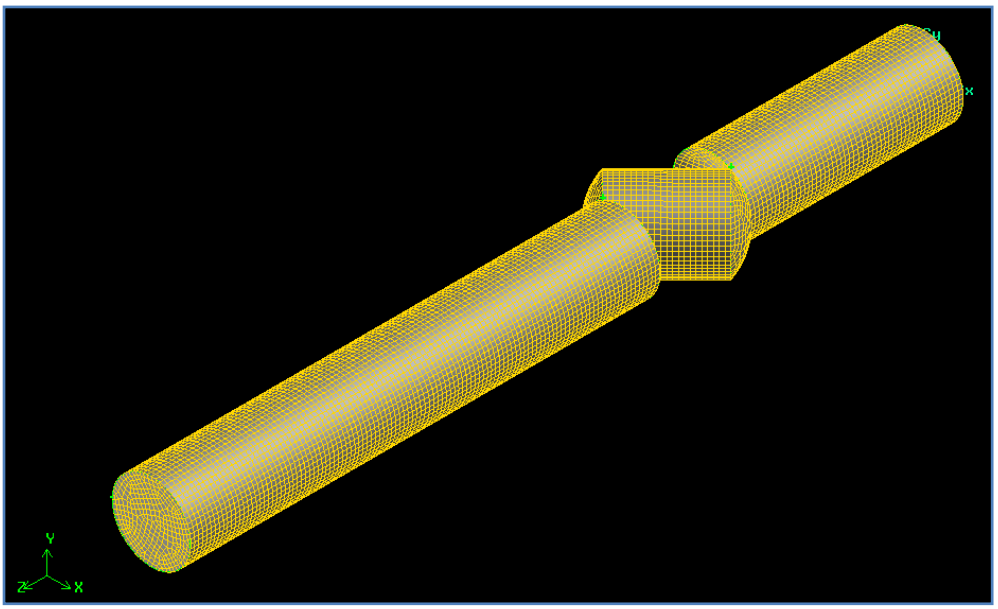

Figure 4: Mesh of the domain in GAMBIT software

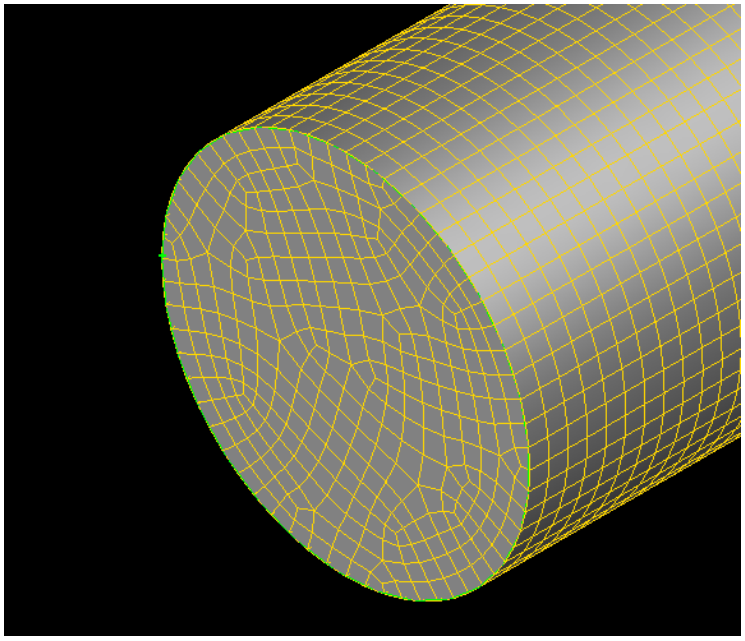

Figure 5: Close view for the mesh.

The next step is to adopt the mesh in FLUENT. The boundary adaption was used to increase the cells near the walls and reduce the difference in volumes. The volume adaption was limited to 1.5 as clear in figures 6 and 7.

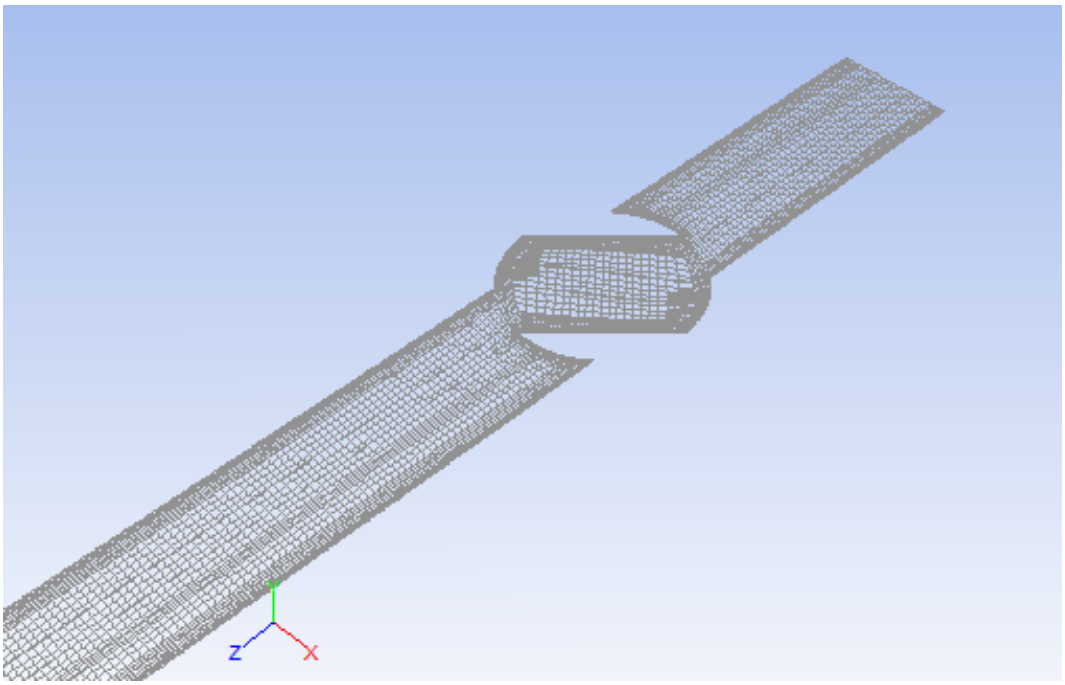


Figure 6: Mesh after adaption for a plane in X-Z

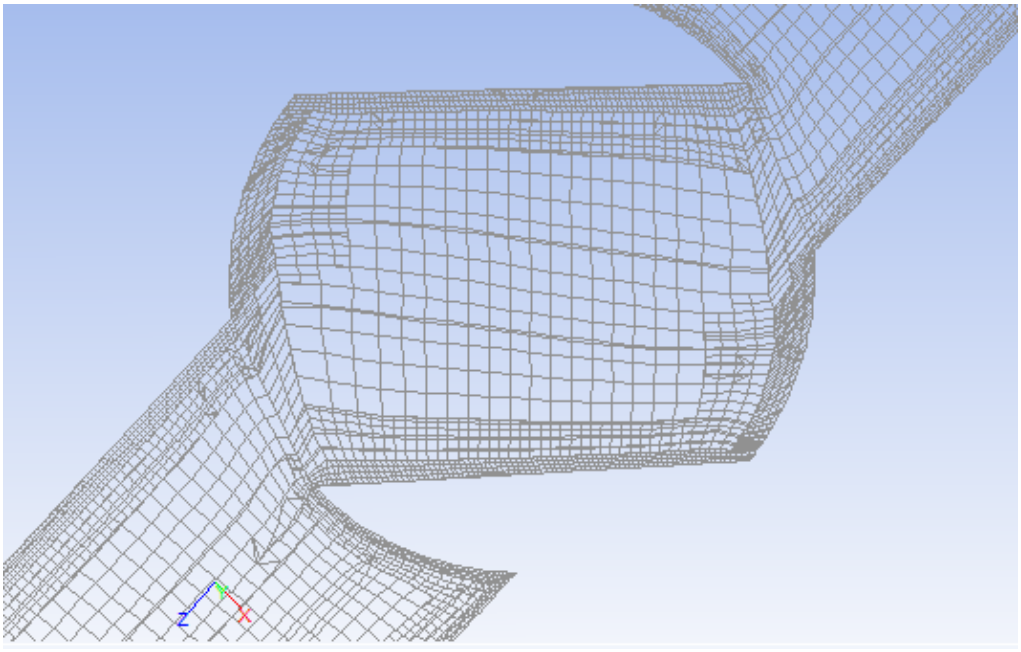

Figure 7: Close view for the mesh after adaption for a plane in X-Z

## 4.3 Fluent Setup

Nowadays, a number of commercial CFD codes have become available. FLUENT is considered to be one of the modern CFD programs for modeling flow, mass and heat transfer problems. It is written in the *C* computer language and it has a number of characteristics such as accuracy, efficient meshing, high speed, and powerful visualization capability. In this section, the available numerical models and solution techniques in FLUENT software which are related to this study are briefly described. More details are available in the reference [Fluent 6.3 user's manual].

### 4.3.1 Boundary Conditions

The following boundary conditions are used to solve the problem:

- **Inlet**

The temperature, velocity, turbulence intensity, and operating pressure are used to identify the inlet conditions.

The Intensity and Hydraulic Diameter is used to identify the condition of turbulence based on the following equations;

$$I = 0.16 (Re_{DH})^{-1/8} \quad (4.3.1)$$

Where $Re_{D_H}$ is the Reynolds number

$$Re_{D_H} = \frac{\rho V D_H}{\mu} \quad (4.3.2)$$

The operating pressure of the model was set at the inlet of the domain so it is used to identify the pressure at the inlet.

- **Outlet**

The outflow option in FLUENT is used to set the boundary conditions of outlet stream.

- **Walls**

All wall conditions are set as an adiabatic with no slip condition and have no thickness.

### 4.3.2 Modelling of Turbulent Flow

There are a number of choices for turbulence models in FLUENT

- Spalart-Allmaras model
- k- ε models
    - Standard k- ε model
    - Renormalization-group (RNG) k- ε model
    - Realizable k- ε model
- K-ω models
    - Standard K-ω model
    - Shear-stress transport (SST) K-ω model
- $v^2 - f$ model (addon)
- Reynolds stress model (RSM)
    - Linear pressure-strain RSM model
    - Quadratic pressure-strain RSM model
    - Low-Re stress-omega RSM model
- Detached eddy simulation (DES) model
    - Spalart-Allmaras RANS model
    - Realizable k- ε RANS model
    - SST k-ω RANS model
- Large eddy simulation (LES) model
    - Smagorinsky-Lilly subgrid-scale model
    - WALE subgrid-scale model

- Kinetic-energy transport subgrid-scale model

As mentioned in chapter 3, the focus of current study will be on four models as follows:

- **Standard k-ε model**

Standard k-ε model is widely used; it solves the equations of turbulent kinetic energy and its rate of dissipation. Its main pros are a stable calculation and logical results for many flows, especially with flows of a high Reynolds number. It is not recommended for highly swirling flows, round jets, or for flows with strong flow separation.

The transport equation of turbulence kinetic energy, *k*

$$\frac{\partial}{\partial t}\ (\rho k) + \frac{\partial}{\partial x_i}\ (\rho k u_i) = \frac{\partial}{\partial x_j}\left[\left(\mu + \frac{\mu_t}{\sigma_k}\right)\frac{\partial k}{\partial x_j}\right] + G_k - \rho\epsilon \qquad (4.3.3)$$

The transport equation of rate of dissipation, *ε*

$$\frac{\partial}{\partial t}\ (\rho\epsilon) + \frac{\partial}{\partial x_i}\ (\rho\epsilon u_i) = \frac{\partial}{\partial x_j}\left[\left(\mu + \frac{\mu_t}{\sigma_\epsilon}\right)\frac{\partial \epsilon}{\partial x_j}\right] + G_{1\epsilon}\ \frac{\epsilon}{k}\ G_k - C_{2\epsilon}\rho\frac{\epsilon^2}{k} \qquad (4.3.4)$$

Where $G_k$ represents the generation of turbulence kinetic energy due to the mean velocity gradients,

$$G_k = -\overline{\rho u_i' u_j'}\frac{\partial u_j}{\partial x_i} \qquad (4.3.5)$$

The turbulent or eddy viscosity, $\mu_t$ , is computed by combining *k* and *ε* as follows:

$$\mu_t = \ \rho C_\mu\ \frac{k^2}{\epsilon} \qquad (4.3.6)$$

$C_{1\epsilon}$, $C_{2\epsilon}$, and $C_{3\epsilon}$ are constants. $\sigma_k$ and $\sigma\epsilon$ are the turbulent Prandtl numbers for *k* and ϵ, respectively.

The model constants:

$$C_1\epsilon = 1.44,\ C_2\epsilon = 1.92,\ C_\mu = 0.09,\ \sigma_k = 1.0,\ \sigma_\epsilon = 1.3$$

- **The RNG k-ε Model**

It is a modified version of the k-ε model. It includes the following modifications: "it has an additional term in its equation that significantly improves the accuracy for rapidly strained flows; the effect of swirl on turbulence is included; it provides an analytical formula for turbulent Prandtl numbers; and it provides an analytically-derived differential formula for effective viscosity that accounts for low-Reynolds-number effects" (Fluent user's manual). This model provides improved results for swirling flows and flow separation. It is not well appropriate for round jets, and is not as stable as the standard k-ε model.

The transport equations of turbulence kinetic energy and rate of dissipation are similar to standard model; however, the main difference between the RNG and standard *k-ε* models is in the additional term in the *ε* equation given by

$$\frac{\partial}{\partial t}(\rho\epsilon) + \frac{\partial}{\partial x_i}(\rho\epsilon u_i) = \frac{\partial}{\partial x_j}\left(\alpha_\epsilon \mu_{eff}\frac{\partial\epsilon}{\partial x_j}\right) + C_{1\epsilon}\frac{\epsilon}{k} + G_k - C_{2\epsilon}\rho\frac{\epsilon^2}{k} - R_\epsilon \qquad (4.3.7)$$

$$R_\epsilon = \frac{C_\mu \rho\eta^3\left(1-\frac{\eta}{\eta o}\right)}{1+\beta\eta^3}\frac{\epsilon^2}{k} \qquad (4.3.8)$$

where

$$\eta \equiv Sk/\varepsilon, \quad \eta o = 4.38, \quad \beta = 0.012$$

For low Reynolds number region the turbulent viscosity is calculated by the following equation:

$$d\left(\frac{\rho^2 k}{\sqrt{\epsilon\mu}}\right) = 1.72\,\frac{\hat{\nu}}{\sqrt{\hat{\nu}^3 - 1 + C_\nu}}\,d\hat{\nu} \tag{4.3.9}$$

Where

$$\hat{\nu} = \frac{\mu_{eff}}{\mu} \tag{4.3.10}$$

$$C_\nu \approx 100$$

For high Reynolds number region, it is calculated as for standard model with a value of 0.0845 for the $C_\mu$ constant.

The Swirl Modification is calculated through the following equation:

$$\mu_t = \mu_{to}\, f\left(\alpha_s, \Omega, \frac{k}{\epsilon}\right) \tag{4.3.11}$$

Where $\mu_{to}$ is the value of turbulent viscosity calculated without the swirl modification and calculated by using equation (4.3.9). $\Omega$ is a characteristic swirl number evaluated within FLUENT, and $\alpha_s$ is a swirl constant. For mildly swirling flows (the default in FLUENT), $\alpha_s$ is set to 0.07.

The inverse effective Prandtl numbers, $\alpha_k$ and $\alpha_Z$ are computed using the following formula:

$$\left|\frac{\alpha - 1.3929}{\alpha_o - 1.3929}\right|^{0.6321} \left|\frac{\alpha + 2.3929}{\alpha_o + 2.3929}\right|^{0.3679} = \frac{\mu_{mol}}{\mu_{eff}} \qquad (4.3.12)$$

Where $\alpha_0 = 10$ and with high-Reynolds-number $\alpha_k = \alpha_\varepsilon \approx 1.393$.

The model constants are set as:

$$C_{1\varepsilon} = 1.42, C_{2\varepsilon} = 1.68$$

- **Realizable k-ε model**

This is another modified version of the k-ε model. A new formulation for the turbulent viscosity and transport equation for the dissipation rate are included. The realizable k-ε model can calculate the flow in round jets and it is also well suitable for swirling flows and flows which involve separation.

The transport equation of turbulence kinetic energy, $k$

$$\frac{\partial}{\partial t}(\rho k) \frac{\partial}{\partial x_j}(\rho k u_j) = \frac{\partial}{\partial x_j}\left[\left(\mu + \frac{\mu_t}{\sigma_k}\right)\frac{\partial k}{\partial x_j}\right] + G_k - \rho\epsilon \qquad (4.3.13)$$

The transport equation of rate of dissipation, $\varepsilon$

$$\frac{\partial}{\partial t}(\rho\epsilon) + \frac{\partial}{\partial x_j}(\rho\epsilon u_j) = \frac{\partial}{\partial x_j}\left[\left(\mu + \frac{\mu_t}{\sigma_k}\right)\frac{\partial \epsilon}{\partial x_j}\right] + \rho C_1 S\epsilon - \rho C_2 \frac{\epsilon^2}{k+\sqrt{\nu\epsilon}} + C_{1\epsilon}\frac{\epsilon}{k}C_{3\epsilon} \qquad (4.3.14)$$

Where $C_1 = Max\left[0.43, \frac{\eta}{\eta+5}\right],\ \eta = S\frac{K}{\epsilon},\ S = \sqrt{2S_{ij}S_{ij}}$

The turbulent viscosity is calculated as for the standard K-ε model; however, the difference between them is in that $C_\mu$ is not a constant. It is computed from

$$C_\mu = \frac{1}{A_o + A_s\frac{kU^*}{\epsilon}} \tag{4.3.15}$$

Where

$$U^* \equiv \sqrt{S_{ij}S_{ij} + \widetilde{\Omega}_{ij}\widetilde{\Omega}_{ij}} \tag{4.3.16}$$

and

$$\widetilde{\Omega}_{ij} = \Omega_{ij} - 2\epsilon_{ijk}\omega_k \tag{4.3.17}$$

$$\Omega_{ij} = \overline{\Omega_{ij}} - \epsilon_{ijk}\omega_k \tag{4.3.18}$$

Where $\widetilde{\Omega}_{ij}$ is the mean rate-of-rotation tensor viewed in a rotating reference frame with the angular velocity $\omega_k$.

where

$$\phi = \frac{1}{3}\cos^{-1}\left(\sqrt{6W}\right), \qquad W = \frac{S_{ij}S_{jk}S_{ki}}{\tilde{S}^3},$$
$$\tilde{S} = \sqrt{S_{ij}S_{ij}}, \quad S_{ij} = \frac{1}{2}\left(\frac{\partial u_j}{\partial x_i} + \frac{\partial u_i}{\partial x_j}\right)$$

And the other model constants are

$$C_1\epsilon = 1.44,\ C_2 = 1.9,\ \sigma_k = 1.0,\ \sigma\epsilon = 1.2$$

$$A_0 = 4.04,\ A_s = \sqrt{6}\cos\phi$$

**Modelling Turbulent Production in the k-ε Models**

$$G_k = -\rho\overline{u_i' u_j'}\frac{\partial u_j}{\partial x_i} \tag{4.3.19}$$

To evaluate $G_k$ in a manner consistent with the Boussinesq hypothesis,

$$G_k = \mu_t S^2 \tag{4.3.20}$$

where $S$ is the modulus of the mean rate-of-strain tensor, defined as

$$S \equiv \sqrt{2S_{ij}S_{ij}} \tag{4.3.21}$$

**Modelling of turbulent heat transport in the *k-ϵ* Models**

The energy equation is given by the following:

$$\frac{\partial}{\partial t}(\rho E) + \frac{\partial}{\partial x_i}\left[u_i\left(\rho E + p\right)\right] = \frac{\partial}{\partial x_j}\left(k_{eff}\frac{\partial T}{\partial x_j} + u_i\left(\tau_{ij}\right)_{eff}\right) \tag{4.3.22}$$

Where $E$ is the total energy, $k_{eff}$ is the effective thermal conductivity, and $\left(\tau_{ij}\right)_{eff}$ is the deviatoric stress tensor, defined as:

$$\left(\tau_{ij}\right)_{eff} = \mu_{eff}\left(\frac{\partial u_j}{\partial x_i} + \frac{\partial u_i}{\partial x_j}\right) - \frac{2}{3}\mu_{eff}\frac{\partial u_k}{\partial x_k}\delta_{ij} \tag{4.3.23}$$

The term involving $\left(\tau_{ij}\right)_{eff}$ represents the viscous heating.

For the standard and realizable k-ε models, the effective thermal conductivity is given by:

$$k_{eff} = k + \frac{C_p \mu_t}{Pr_t} \quad (4.3.24)$$

where k is the thermal conductivity. The default value of the turbulent Prandtl number is 0.85.

For the RNG k-ε model, the effective thermal conductivity is

$$k_{eff} = \alpha C_p \mu_{eff} \quad (4.3.25)$$

- **Reynolds Stress Model (RSM)**

The most general form of classical turbulence model, with very accurate calculation of mean flow properties and all Reynolds stress for many simple and more complex flows. In this model the isotropic eddy-viscosity hypothesis is ignored and it closes the Reynolds-averaged Navier-Stokes equations by solving transport equations for the Reynolds stresses, together with an equation for the dissipation rate. This resulted in five additional transport equations for 2D flows and seven additional transport equations for 3D.

The transport equation of the Reynolds stresses can be expressed as:

$$\underbrace{\frac{\partial}{\partial t}\left(\rho\overline{u_j'u_j'}\right)}_{\textbf{Local time derivative}} + \underbrace{\frac{\partial}{\partial x_k}\left(\rho u_k\overline{u_i'u_j'}\right)}_{\textbf{Cij} \equiv \textbf{Convection}} = \underbrace{-\frac{\partial}{\partial x_k}\left[\rho\overline{u_i'u_j'u_k'} + p\left(\delta_{kj}u_i' + \delta_{ik}u_j'\right)\right]}_{\textbf{DT,ij} \equiv \textbf{Turbulent diffusion}}$$

$$+ \underbrace{\frac{\partial}{\partial x_k}\left[\mu\frac{\partial}{\partial x_k}\left(u_i'u_j'\right)\right]}_{DL_{ij} \equiv Molecular\ \ diffusion} \underbrace{-\rho\left(\overline{u_i'u_k'}\frac{\partial u_j}{\partial x_k} + \overline{u_j'u_k'}\frac{\partial u_i}{\partial x_k}\right)}_{P_{ij} \equiv Stress\ \ Production} \underbrace{-\rho\beta\left(g_i\overline{u_j'\theta} + g_j\overline{u_i'\theta}\right)}_{G_{ij} \equiv Buoyancy\ \ Production}$$

$$\underbrace{+P\left(\overline{\frac{\partial u_i'}{\partial x_j} + \frac{\partial u_j'}{\partial x_i}}\right)}_{\boldsymbol{\phi ij} \equiv \textbf{Pressure Strain}} - \underbrace{2\mu\overline{\frac{\partial u_i'}{\partial x_k}\frac{\partial u_j'}{\partial x_k}}}_{\boldsymbol{\epsilon_{ij}} \equiv \textbf{Dissipation}} \underbrace{-2\rho\Omega k\left(\overline{u_j'u_m'}\epsilon_{ikm} + \overline{u_i'u_m'}\epsilon_{jkm}\right)}_{F_{ij} \equiv \text{Production by system Rotation}} \tag{4.3.26}$$

**Modelling Turbulent Diffusive Transport in RSM Model**

$$D_{T,ij} = \frac{\partial}{\partial x_k}\left(\frac{\mu_t}{\sigma_k}\overline{\frac{\partial u_i'u_j'}{\partial x_k}}\right) \tag{4.3.27}$$

The turbulent viscosity, $\mu_t$ is computed as for standard K-E model and the value of $\sigma_k$ = 0.82

**Modelling the Pressure-Strain Term in RSM Model**

The pressure-strain term, $\phi_{ij}$ can be modeled by using three relations: Linear Pressure-Strain Model, Quadratic Pressure-Strain Model, Low-Re Stress-Omega Model. However, in this study the Linear Pressure-Strain model is used where enhanced wall treatment is available.

$\phi_{ij}$ can be modeled by uses the following breakdown:

$$\phi_{ij} = \phi_{ij,1} + \phi_{ij,2} + \phi_{ij,w} \tag{4.3.28}$$

where $\phi_{ij,1}$ is the slow pressure-strain term, also known as the return-to-isotropy term, $\phi_{ij,2}$ is called the rapid pressure-strain term, and $\phi_{ij,w}$ is the wall-reflection term.

The slow pressure-strain term, $\phi_{ij,1}$ is modeled as

$$\phi_{ij,1} \equiv -C_1\rho\frac{\epsilon}{k}\left[\overline{u_i'u_j'} - \frac{2}{3}\delta_{ij}k\right] \tag{4.3.29}$$

with $C_1$ = 1.8.

The rapid pressure-strain term, $\phi_{ij,2}$ is modeled as

$$\phi_{ij,2} \equiv -C_2\left[(P_{ij} + F_{ij} + G_{ij} + C_{ij}) - \frac{2}{3}\delta_{ij}(P+G-C)\right] \tag{4.3.30}$$

where $C_2$ = 0.60, $P_{ij}$, $F_{ij}$, $G_{ij}$ $and$ $C_{ij}$ are defined as in Equation (4.3.26),

$$P = \frac{1}{2}P_{kk} \quad G = \frac{1}{2}G_{kk} \quad c = \frac{1}{2}c_{kk} \tag{4.3.31}$$

The wall-reflection term,$\phi_{ij,w}$ modeled as

$$\phi_{ij,w} \equiv C_1'\frac{\epsilon}{k}\left(\overline{u_k'u_m'}n_m n_m\delta_{ij} - \frac{3}{2}\overline{u_i'u_k'}n_j n_k - \frac{3}{2}\overline{u_j'u_k'}n_i n_k\right)\frac{C_\ell k^{\frac{3}{2}}}{\epsilon d}$$

$$+ C_2^{'} \left( \phi_{km,2} n_k n_m \delta_{ij} - \frac{3}{2} \phi_{ik,2} n_j n_k - \frac{3}{2} \phi_{jk,2} n_i n_k \right) \frac{C_\ell k^{\frac{3}{2}}}{\epsilon d} \quad (4.3.32)$$

where $C_1^{'} = 0.5, C_2^{'} = 0.3, n_k$ is the $x_k$ component of the unit normal to the wall, $d$ is the normal distance to the wall, and $C_\ell = C_\mu^{3/4}/k$, where $C_\mu$ = 0.09 and $k$ is the von Kármán constant (= 0.4187).

**Modelling the Turbulence Kinetic Energy in RSM Model**

To obtaining the boundary conditions for the Reynolds stresses the transport equation of the turbulence kinetic energy is solved:

$$\frac{\partial}{\partial t}(\rho k) + \frac{\partial}{\partial x_i}(\rho k u_i) = \frac{\partial}{\partial x_j} \left[ \left( \mu + \frac{\mu_t}{\sigma_k} \right) \frac{\partial k}{\partial x_j} \right] + \frac{1}{2} (P_{ii} + G_{ii}) - \rho \epsilon \quad (4.3.33)$$

Where $\sigma_k = 0.82$.

The dissipation tensor, $\epsilon_{ij}$ is modeled as

$$\epsilon_{ij} = \frac{2}{3} \delta_{ij} (\rho \epsilon) \quad (4.3.34)$$

**Modeling the Dissipation Rate in RSM Model**

The scalar dissipation rate $\varepsilon$ is computed with a model transport equation similar to that used in the standard $k$-$\varepsilon$ model:

$$\frac{\partial}{\partial t}(\rho\epsilon) + \frac{\partial}{\partial x_i}(\rho\epsilon u_i) = \frac{\partial}{\partial x_j}\left[\left(\mu + \frac{\mu_t}{\sigma_\epsilon}\right)\frac{\partial \epsilon}{\partial x_j}\right] C_{\epsilon 1}\ \frac{1}{2}\ [P_{ii} + C_{\epsilon 3} G_{ii}]\ \frac{\epsilon}{k} - C_{\epsilon 2}\rho\frac{\epsilon^2}{k} \quad (4.3.35)$$

where $\sigma_\epsilon = 1.0, C_{\epsilon 1} = 1.44,\ C_{\epsilon 2} = 1.92$

$$C_{3\epsilon} = \tanh\left|\frac{v}{u}\right| \quad (4.3.36)$$

**Modelling of turbulent heat transport in RSM Model**

$$\frac{\partial}{\partial t}(\rho E) + \frac{\partial}{\partial x_i}[u_i(\rho E + p)] = \frac{\partial}{\partial x_j}\left[\left(k + \frac{C_p \mu_t}{Pr_t}\right)\frac{\partial T}{\partial x_j} + u_i(\tau_{ij})_{\text{eff}}\right] \quad (4.3.37)$$

where $E$ is the total energy and $(\tau_{ij})_{\text{eff}}$ is the deviatoric stress tensor, defined as

$$(\tau_{ij})_{\text{eff}} = \mu_{\text{eff}}\left(\frac{\partial \mu_j}{\partial x_i} + \frac{\partial \mu_i}{\partial x_j}\right) - \frac{2}{3}u_{\text{eff}}\frac{\partial \mu_k}{\partial x_k}\delta_{ij} \quad (4.3.38)$$

The term involving $(\tau_{ij})_{\text{eff}}$ represents the viscous heating, and is always computed in the density-based solvers. The default value of the turbulent Prandtl number is 0.85.

**Modeling of Enhanced Wall Treatment**

The enhanced wall treatment which includes the two-layer approach identifies $\varepsilon$ and turbulent viscosity in the near-wall cells. The whole domain is divided into a viscous region and a fully-turbulent region. The two regions are separated using a wall-distance-based, turbulent Reynolds number, $\text{Re}_y$ , defined as

$$Re_y \equiv \frac{\rho y \sqrt{k}}{\mu} \tag{4.3.39}$$

where *y* is the normal distance from the wall at the cell centers.

In the fully turbulent region($Re_y > Re_y^*\ Re_y^* = 200$), the *k*-$\varepsilon$ models or the RSM are employed.

In the viscosity-affected near-wall region ($Re_y > Re_y^*$) a one-equation model is employed. In the one-equation model, the momentum equations and the *K* equation are solved as normal. However, the turbulent viscosity, $\mu_{t,}$, is computed from

$$\mu_{t,\ 2\ layer} = \rho C_\mu \ell_\mu \sqrt{k} \tag{4.3.40}$$

where the length scale that appears in the above equation is computed as follows:

$$\ell_\mu = y C_\ell^* \left(1 - e^{-Re_y/A_\mu}\right) \tag{4.3.41}$$

The two-layer formulation for turbulent viscosity described above is used as a part of the enhanced wall treatment, in which the two-layer definition is smoothly blended with the high-Reynolds-number $\mu_t$ definition from the outer region, as follows:

$$\mu_{t,\ enh} = \lambda_\epsilon \mu t + (1 - \lambda_\epsilon)\mu_{t,2\ layers} \tag{4.3.42}$$

Where $\mu_t$ *i*s the high-Reynolds-number definition as described in the *k*-$\varepsilon$ models or the RSM. A blending function, $\lambda_\epsilon$ is defined in such a way that it is equal to unity far from walls and is zero very near to walls. The blending function chosen is:

$$\lambda_\epsilon = \frac{1}{2}\left[1 + \tanh\left(\frac{Re_y - Re_y^*}{A}\right)\right] \tag{4.3.43}$$

The constant $A$ determines the width of the blending function. By defining a width such that the value of $\lambda_\epsilon$ will be within 1% of its far-field value given a variation of $Re_y$, the result is

$$A = \frac{|\Delta\, Re_y|}{\tanh^{-1}(0.98)} \tag{4.3.44}$$

Typically, $\Delta\, Re_y$ would be assigned a value that is between 5% and 20% of $Re_y^*$.

The $\varepsilon$ field is computed from

$$\epsilon = \frac{k}{\ell_\epsilon}^{3/2} \tag{4.3.45}$$

The length scales that appear in the above Equation are solved as follows:

$$\ell_\epsilon = yC_\ell^*\left(1 - e^{-Re_y/A_c}\right) \tag{4.3.46}$$

If the whole flow domain is inside the viscosity-affected region ($Re_y$ <200), $\boldsymbol{\varepsilon}$ is not obtained by solving the transport equation; it is instead obtained algebraically from Equation (4.3.47), FLUENT uses a procedure for the $\boldsymbol{\varepsilon}$ specification that is similar to the $\mu_t$ blending in order to ensure a smooth transition between the algebraically-specified $\boldsymbol{\varepsilon}$ in the inner region and the $\boldsymbol{\varepsilon}$ obtained from solution of the transport equation in the outer region.

The constants in the length scale formulas:

$$C_\ell^* = kC_\mu^{-3/4}, A_\mu = 70, A_\epsilon = 2C_\ell^*$$

### 4.3.3 Solution Strategy

**Numerical Methods of Solver**

There are two numerical methods for solving the flow in FLUENT: pressure-based solver and density-based solver. The pressure-based solver is normally used for incompressible and slightly compressible flows. On the other hand, the density-based approach was initially designed for high-speed compressible flows. The two numerical methods use a similar discretization process; however, the approach which is used to linearize and solve the discretized equations is different (see Figures 8 & 9).

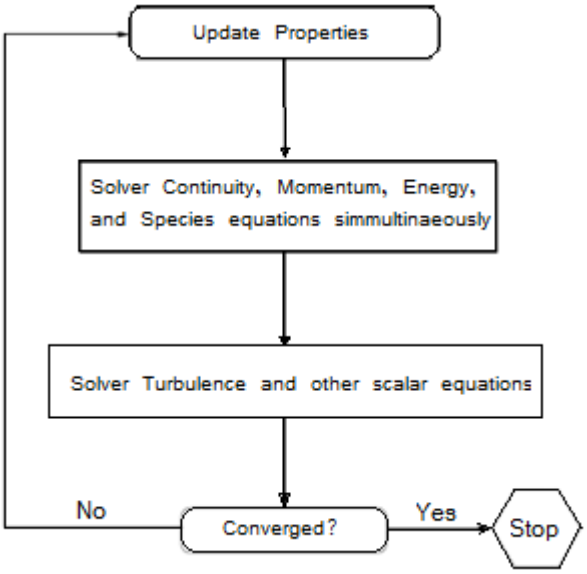


Figure 8: Overview of the density-based solution method [Fluent 6.3 user's manual]

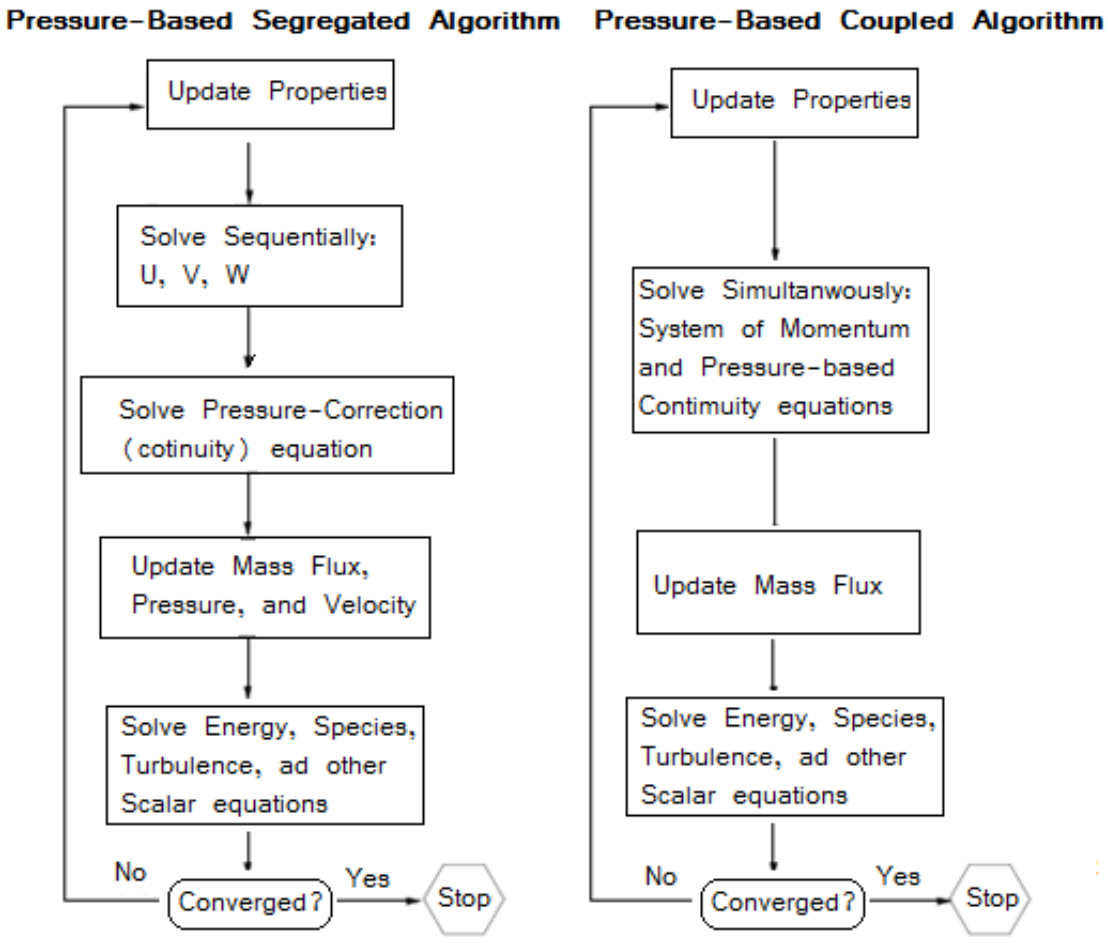


Figure 9: Overview of the pressure-based solution methods [Fluent 6.3 user's manual]

In this study, the pressure-based segregated algorithm method is used. In the pressure-based solver, an implicit form is taken with respect to the variable when the governing equations are linearized. For each variable, the existing and unknown values from neighboring cells are used to calculate the unknown value in each cell.

**Discretization of Scalar Transport Equation**

Discretization of the governing equations can be shown by the following equations for a scalar quantity $\phi$ and an arbitrary control volume *V*:

$$\int_v \frac{\partial \rho \phi}{\partial t}\, dV + \oint \rho \phi \vec{v}.d\vec{A} = \oint \Gamma_\phi \nabla_\phi . d\vec{A} + \int_V S_\phi D_V \qquad (4.3.47)$$

Where

ρ = Density

$\vec{v}$ = Velocity vector

$\vec{A}$ = surface area vector

$\Gamma\phi$ = Diffusion coefficient for $\phi$

$\nabla\phi$ = Gradient of $\phi$

$S\phi$ = Source of $\phi$ per unit volume

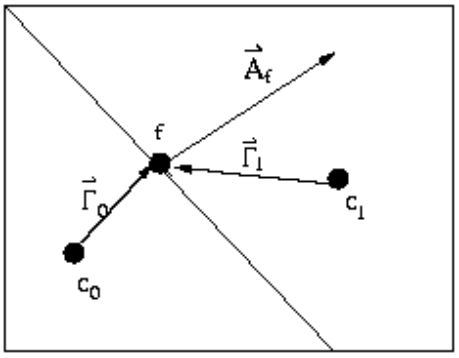


Figure 10. Control Volume Used to Illustrate Discretization of a Scalar Transport Equation

The Discretization of the above equation is illustrated in the following equation:

$$\frac{\partial \rho \phi}{\partial t} V + \sum_f^{N_{faces}} \rho_f \vec{v}_f \phi_f . \vec{A}_f = \sum_f^{N_{faces}} \Gamma_\phi \nabla \phi_f . \vec{A}_f + S_\phi V \qquad (4.3.48)$$

Where

$N_{faces}$ = Number of faces enclosing cell

$\phi_f$ = Values of ϕ convected through face $f$

$\rho_f \vec{v} f . \vec{A}_f$ = Mass flux through the face

$\vec{A}_f$ = Area of face $f$

$\nabla \phi_f$ = Gradient of ϕ at face $f$

V = Cell volume

**Solving the Linear System**

A linearized form of Equation (4.3.48) can be written as

$$\alpha p \phi = \sum_{nb} \alpha_{nb} \phi_{nb} + b \qquad (4.3.49)$$

where the subscript $nb$ refers to neighbor cells, and $\alpha p$ and $\alpha_{nb}$ are the linearized coefficients for $\phi$ and $\phi_{nb}$.

**Spatial Discretization Schemes**

As explained previously, the control-volume-based technique converts a general scalar transport equation to an algebraic equation that can be solved numerically. In a pressure based solver, there are five spatial discretization schemes: First-Order upwind, Second-Order upwind, QUICK, Third-order MUSCL, and Power law. The First-Order upwind is used in this study.

**Evaluation of Gradients and Derivatives**

There are three options in FLUENT for computing the gradients and derivatives. These options are; Green-Gauss Cell Based, Green-Gauss Node Based, and Least Squares Cell Based. Green-Gauss Cell Based method is used in this study.

To compute the gradient of the scalar $\phi$ at the cell center $c0$, the discrete Green-Gauss Cell Based scheme can be formed as:

$$(\nabla\phi)c0 = \frac{1}{v}\sum_f \bar{\phi}_f \vec{A}_f \tag{4.3.50}$$

where $\bar{\phi}_f$ is the value of $\phi$ at the cell face centroid.

The face value $\bar{\phi}_f$ is taken from the arithmetic average of the values at the neighbouring cell centres:

$$\bar{\phi}_f = \frac{\phi_{c0} + \phi_{c1}}{2} \tag{4.3.51}$$

**Pressure-Velocity Coupling Methods**

In the pressure-based approach, the velocity field is obtained from the momentum equations and the pressure field is determined by solving a pressure or pressure correction equation, which is obtained by manipulating continuity and momentum equations. Four different pressure-velocity algorithms are available for the segregated solver: SIMPLE, SIMPLEC, PISO and Fractional Step. The SIMPLE algorithm which is used in the current study uses a relationship between velocity and pressure corrections to enforce mass conservation and to obtain the pressure field.

**Pressure Interpolation Schemes**

The default standard scheme in FLUENT is to use momentum equation coefficients to interpolates the pressure values at the faces. However, four other alternative methods are also available: the linear scheme, the second-order scheme, the body-force-weighted scheme, and the PRESTO. In this study, the standard scheme is used.

**Under-Relaxation control of Variables**

Because of the nonlinearity of the equations solved by the CFD software, it is necessary to control the change of $\phi$ variable. The following equation shows the control scheme of variable value:

$$\emptyset = \emptyset_{old} + \alpha\Delta\emptyset \tag{4.3.52}$$

Where $\emptyset_{old}$ is the old value of the variable, $\alpha$ is the under-Relaxation factor

The following table shows the set values for the Under-relaxation of variables:

**Table 2: Under-relaxation of variables**

| | |
|---|---|
| Pressure | 0.3 |
| Density | 1 |
| Body Force | 1 |
| Momentum | 0.7 |
| Turbulent Kinetic Energy | 0.8 |
| Turbulent Viscosity | 1 |
| Turbulent Dissipation Rate | 0.8 |
| Reynolds Stresses | 1 |
| Energy | 1 |

# CHAPTER 5

## RESULTS & DISCUSSION

In this study a number of key issues which are related to the flow behavior and entropy generation at a ball valve, were investigated. These issues in brief are; studying different turbulent flow models, effect of upstream velocity, effect of upstream temperature, effect of upstream pressure, and effect of valve position.

### 5.1 Comparison between Turbulent Flow Models

Four turbulent flow models were used to investigate the impact of upstream conditions on the flow and irreversibility at a ball valve. These turbulent flow models are:

1. Standard $k$-$\varepsilon$ model,
2. Realizable $k$-$\varepsilon$ Model,
3. RNG $k$-$\varepsilon$ Model,
4. Reynolds Stresses Model.

The comparison is based on the velocity profiles, pressure profiles, and the turbulence intensity profiles. Moreover, other maximum and minimum values of velocity and pressure were compared. The valve's assumed operating conditions are illustrated in figure 11.

Water

@

$T_i$ = 300 K

Throttling valve

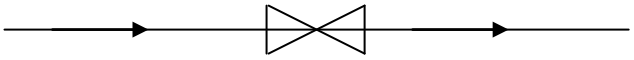

$P_i$ = 2 Absolute bar

$\theta = 45^{o}$

$V_i$ = 2 m/s

Figure 11: Upstream conditions and valve position for the comparison between different turbulent flow models

### 5.1.1 Velocity Profile

The predicted velocity profiles at X-Z plane using the four turbulent models are shown in figure 12a, 12b, 12c, and 12d.

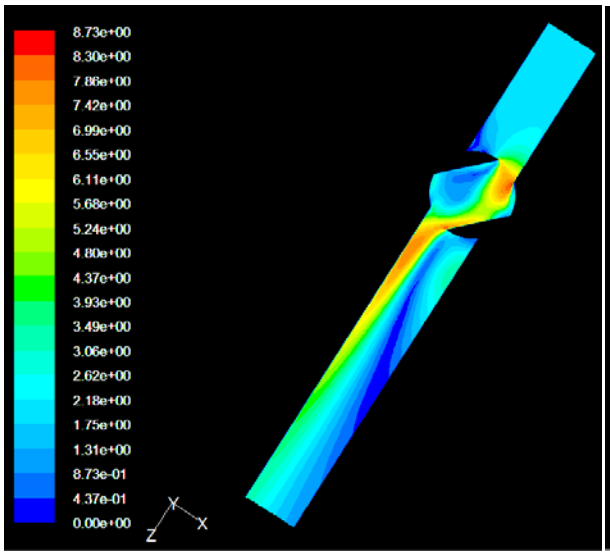


Figure 12a: Velocity profile using Standard *k-ε* model

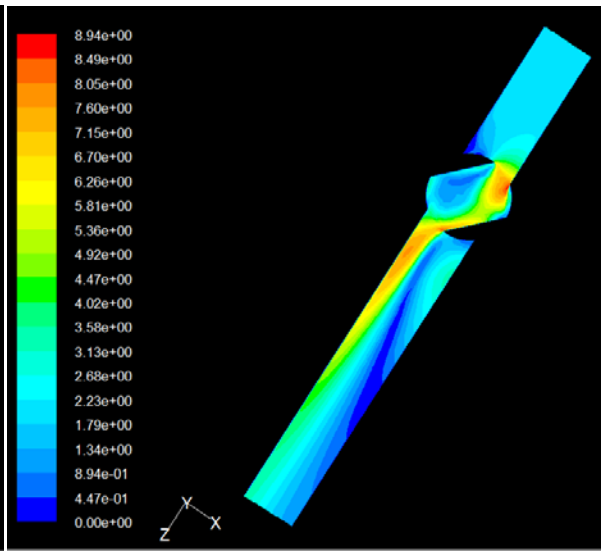


Figure 12b: Velocity profile using Realizable *k-ε* Model.

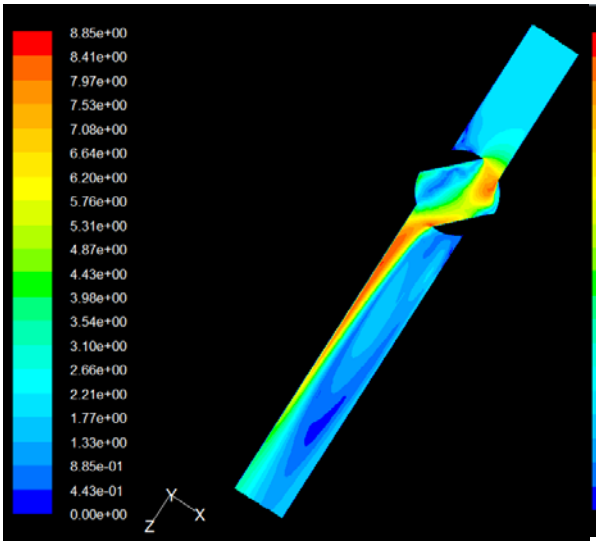


Figure 12c: Velocity profile using RNG *k-ε* Model

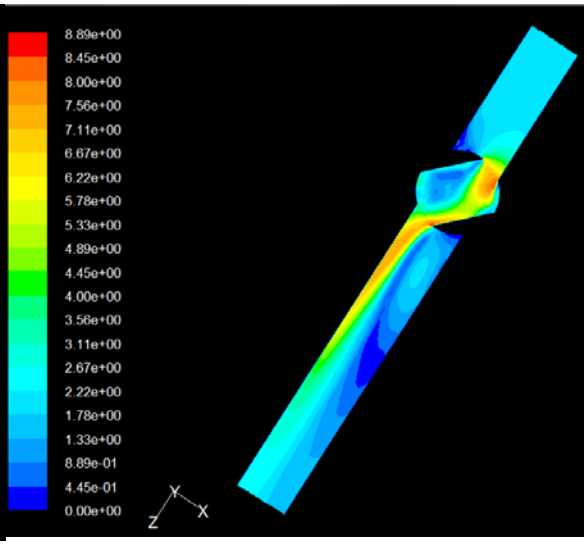


Figure 12d: Velocity profile using RS Model.

It was observed that the velocity profiles of the Standard *k-ε* model (figure 12a), Realizable *k-ε* model (figure12b), and RS model (figure 12d) are more or less having the same velocity gradient as well as the maximum and minimum velocity locations. Meanwhile, the profile of RNG *k-ε* model (figure 12c) is different. It was also found that the circulation areas in all obtained results are at the valve area and the outlet pipe, moreover these areas are almost the same in Standard *k-ε* model (figure 12a) and Realizable *k-ε* model (figure 12b).

### 5.1.2 Absolute Static Pressure Profile

The absolute static pressure profiles at X-Z plane predicted by the four turbulent models are shown in figures 13a, 13b, 13c, and 13d.

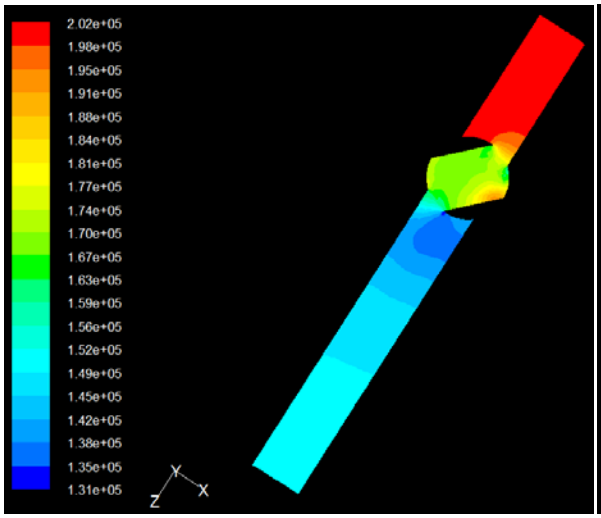


Figure 13a: Absolute static pressure profile using Standard *k-ε* model

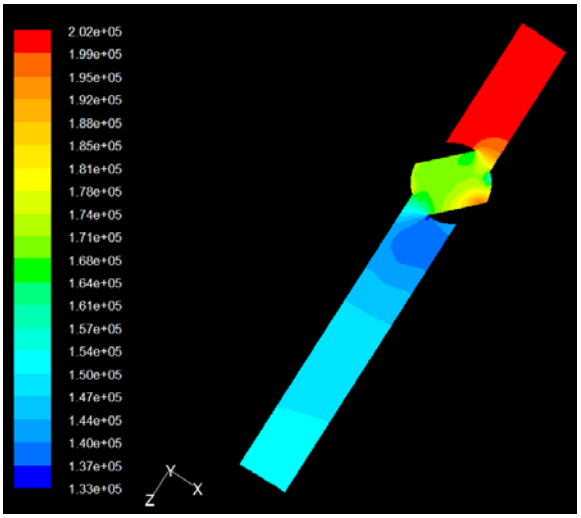


Figure 13b: Absolute static pressure profile using Realizable *k-ε* Model

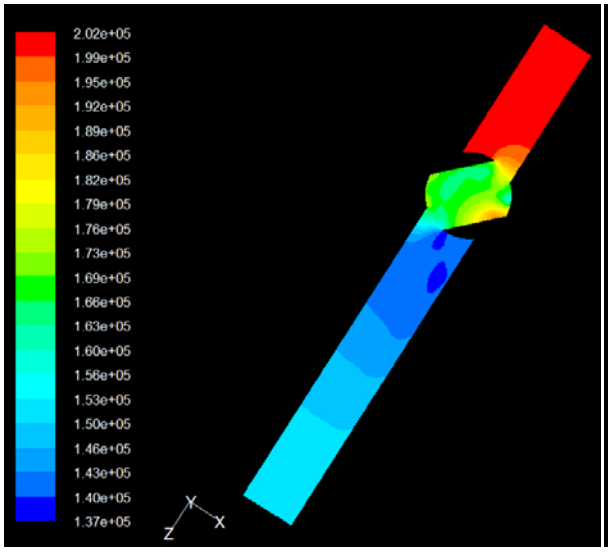


Figure 13c: Absolute static pressure profile using RNG *k-ε* Model

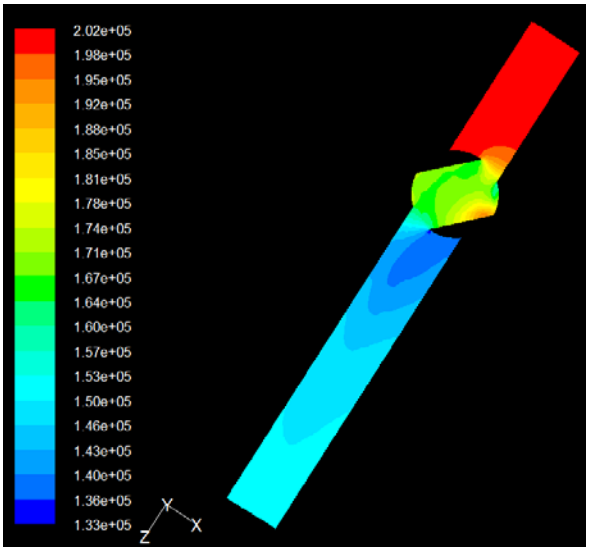


Figure 13d: Absolute static pressure profile using RS Model

It was found that the static pressure profiles of the four models are almost the same. The lowest static pressure was observed to occur at the outlet edge of the valve which might be the area of the cavitation if any.

### 5.1.3 Turbulence Intensity

The turbulence Intensity predicted at X-Z plane by the four turbulent models are shown in figures 14a, 14b, 14c, and 14d.

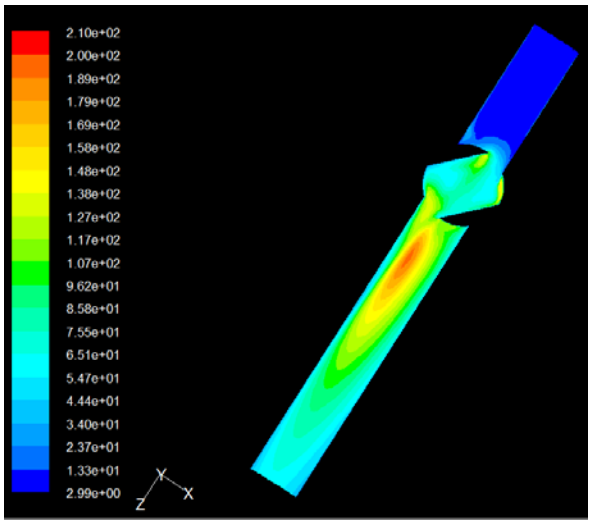


Figure 14a: Turbulence intensity profile using Standard *k-ε* model

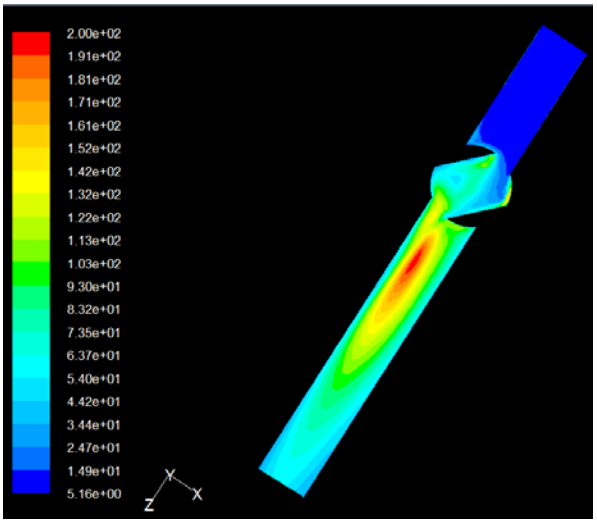


Figure 14b: Turbulence intensity profile using Realizable *k-ε* Model.

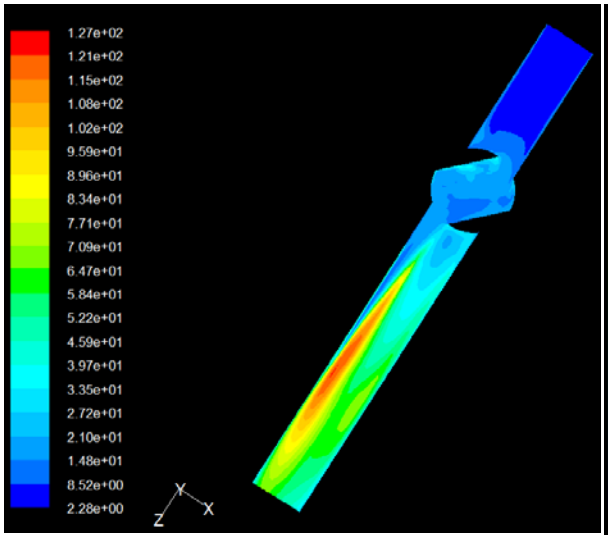


Figure 14c: Turbulence intensity profile using RNG *k-ε* Model

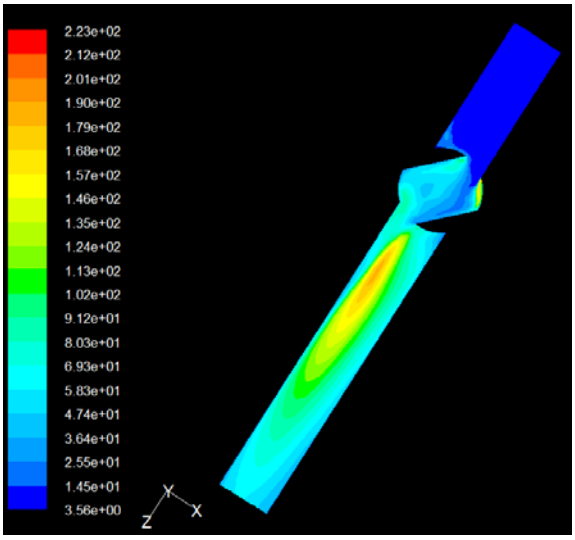


Figure 14d: Turbulence intensity profile using RS Model

From the figures 14a, 14b, 14c, and 14d, it was found that the turbulence intensities predicted by the four models are different. This difference is attributed to the variation of assumptions considered in each model.

### 5.1.4 Maximum and Minimum Values

The predicted maximum local velocities are presented in figure 15. The predicted maximum local velocities of the four turbulent models are to some extent comparable, ranges between 8.72 and 8.97 m/s. The percentage deviation between the maximum and minimum predicted local velocity does not exceed 3 percent.

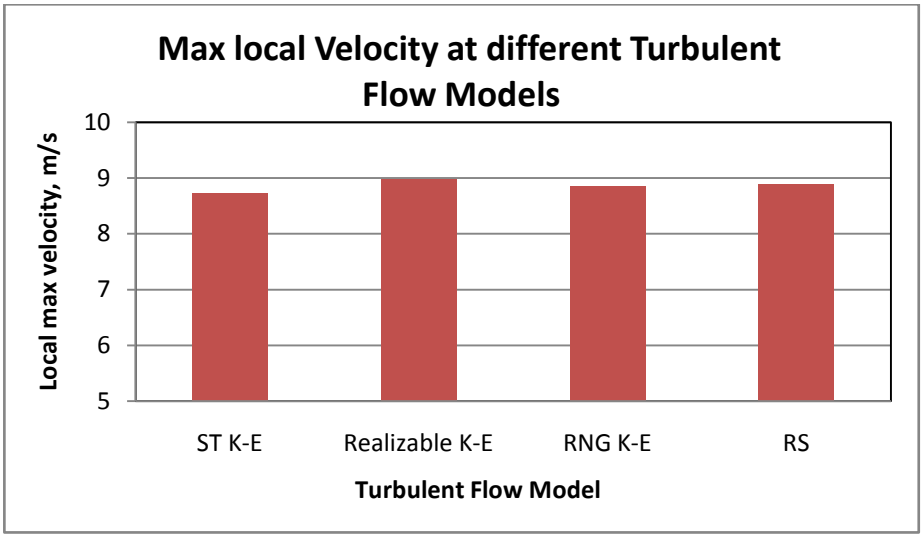


Figure 15: Maximum local velocity predicted by different turbulent models.

Figure 16 shows the magnitude of maximum and minimum local absolute pressure across the valve. It was noticed that there was no significant difference between the four turbulent models values.

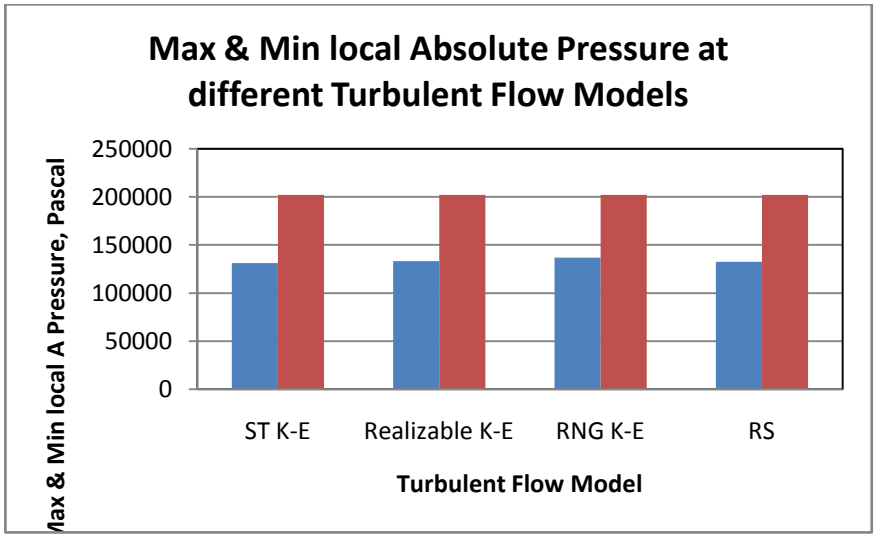


Figure 16: Maximum and minimum local absolute static pressure predicted by different turbulent models

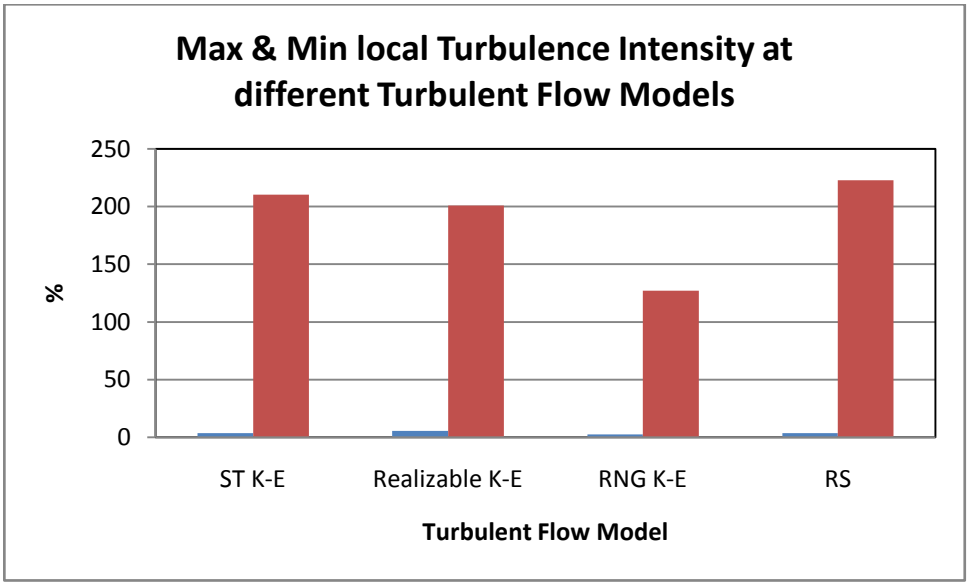


Figure 17: Maximum and minimum local turbulence intensity at different turbulent models.

It was also observed that the turbulence intensity values predicted by the Standard *k*-*ε*, Realizable *k*-*ε*, and RS models are nearly the same while it is less for the RNG *k*-*ε* model, see figure 17.

Across the center line of the pipe along with the valve, the axial velocity and the absolute static pressure are presented in figure 18 and 19, respectively. It is clear that the velocity and pressure profiles for the four turbulent models are the same except for the velocity profile of RNG *k*-*ε* model after the valve outlet in pipe length range of 0.3 to 0.75 m.

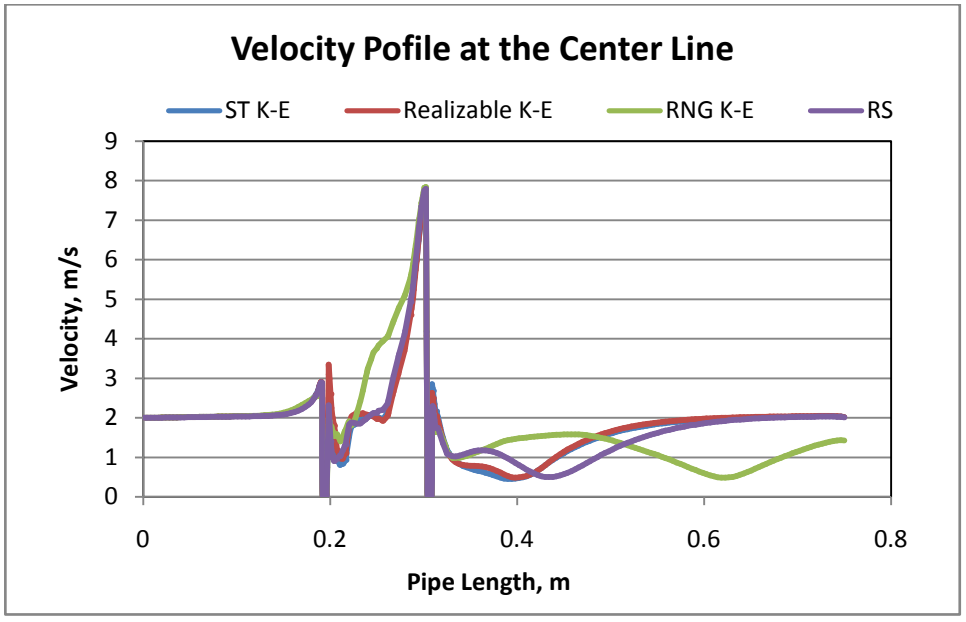


Figure 18: Velocity profile at the center line of domain at different turbulent models

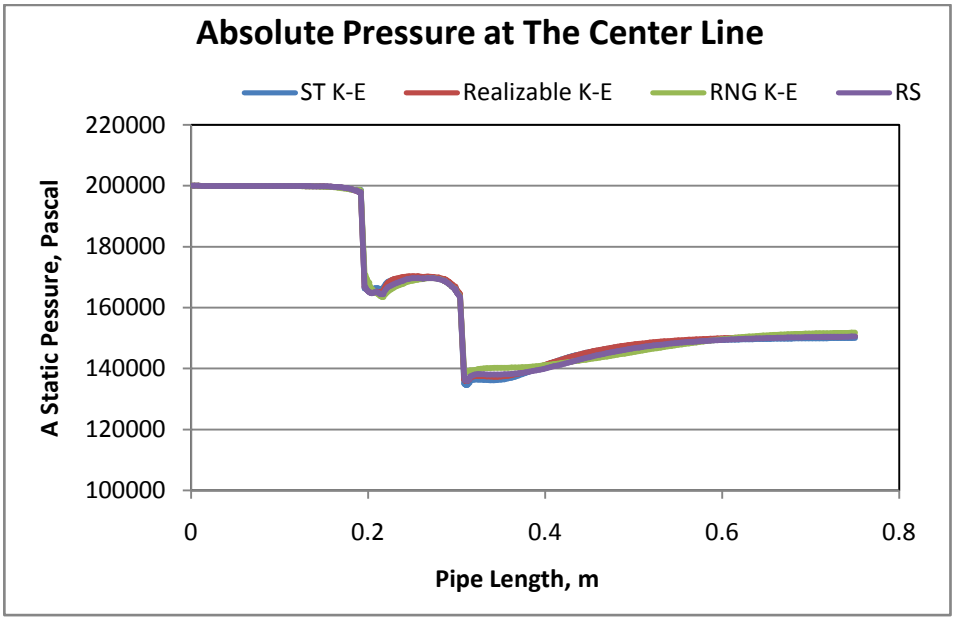


Figure 19: Absolute static pressure at the center line of domain at different turbulent models

### 5.1.5 Pressure Drop

The difference of the absolute static pressure between the pipe inlet and outlet was calculated to explore the effect of the presence of valve on the pressure drop. It was noticed that the pressure drop for all models ranges between 48,262 to 50,006 Pa and the Realizable *k-ε* and Reynolds Stresses models have the same value of 49,400 Pa, see figure 20.

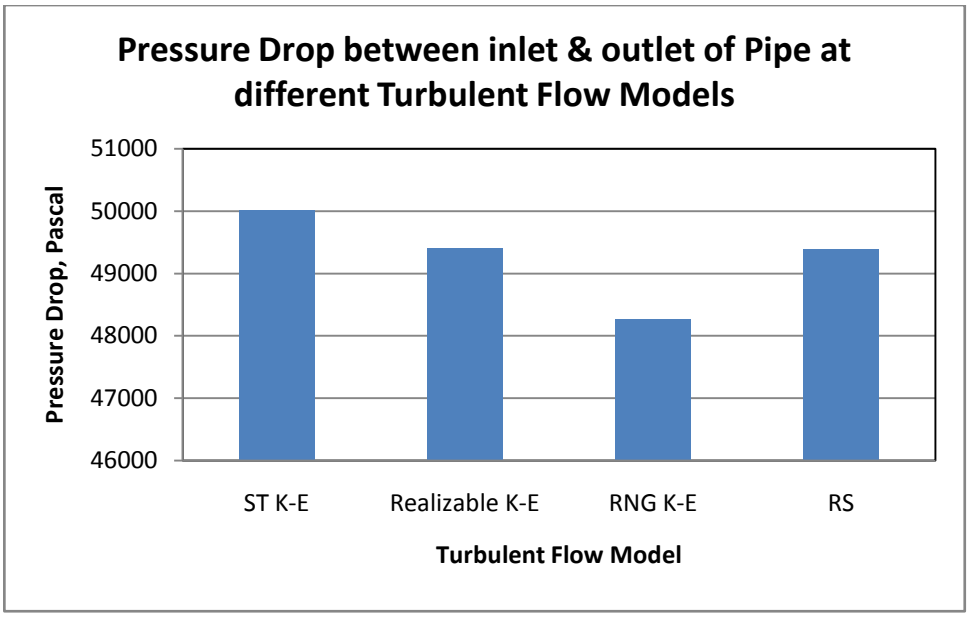


Figure 20: Pressure drop between inlet and outlet of the pipe at different turbulent models

From the previous analysis, it was found that Standard *k-ε*, Realizable *k-ε*, and Reynolds Stresses models are giving more or less the same results while the RNG *k-ε* model is

predicting slightly different profiles and values. This might be due to the effect of swirl modification in the RNG $k$-$\varepsilon$ model.

Despite the complexity and the high computing time of Reynolds Stresses model, it highly recommended to be used for complex flow at throttling devices such as orifices and valves (S. Eiamsa-ard, 2008). In the following sections all results are obtained on the basis of the Reynolds Stresses model.

## 5.2 The Flow Characteristics and Entropy Generation

The design of valve requires specifying a number of variables such as the maximum local velocity, static pressure, cavitation index, loss coefficient, flow coefficient, etc. In this section the effects of upstream velocity, pressure, and temperature, as well as valve position are investigated.

### 5.2.1 Effect of Upstream Velocity

Four different inlet velocities were examined to explore their effect on the flow behavior. The velocity values used in this study are 1, 2, and 3 m/s, the fluid is water at temperature of 300K, the valve position is at 45 degree and the inlet pressure is at 2 A.bar as shown in figure 21.

Water @ $T_i$ = 300 K

Throttling valve

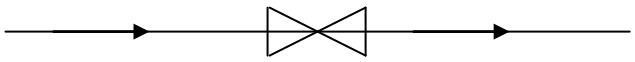

$P_i$ = 2 Absolute bar

$V_i$ = 1, 2, 3 m/s

$\theta = 45^{o}$

Figure 21: Upstream conditions and valve position used to study the effect of upstream velocity

Figure 22 reveals that increasing the inlet velocity result in a linear increase of the maximum local velocity. The increase of upstream velocity from 1 to 3 m/s increases the maximum local velocity from 4 to 13.35 m/s. From the previous section it was noticed that the high local velocity was near the edges of the valve. This might help the designers in choosing the proper material to avoid material deterioration which might be caused by erosion problems if the slip conditions are considered.

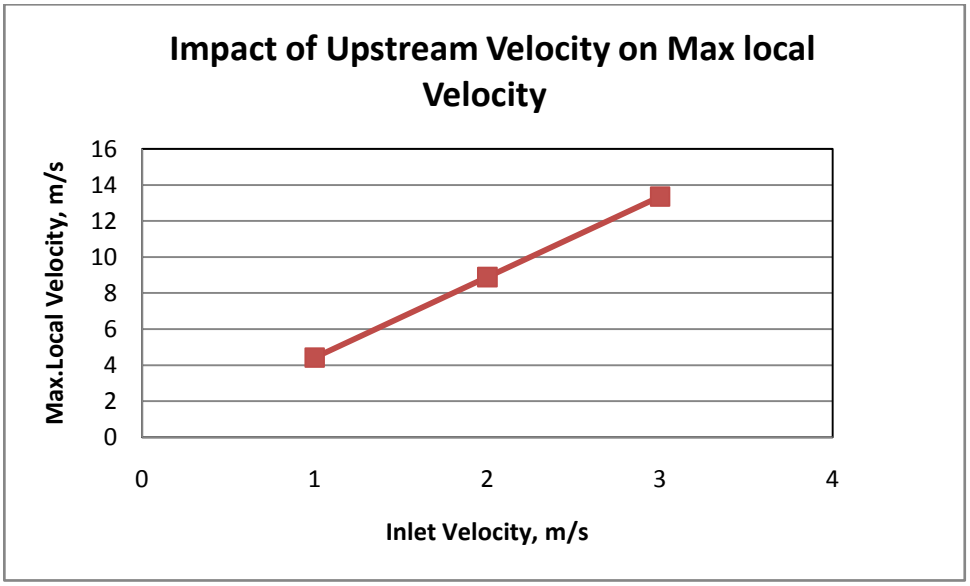


Figure 22: Maximum local velocity values at different inlet velocity.

The increase of pressure drop due to the increase of inlet velocity is inevitable issue. This deterioration in energy is due to the irreversibility by frictional losses between the fluid and walls and between the fluid layers. The increase of upstream velocity from 1 to 3 m/s causes an increase in the pressure drop from 12.3 to 111 kPa and it is nearly linear as shown in the above figure 23.

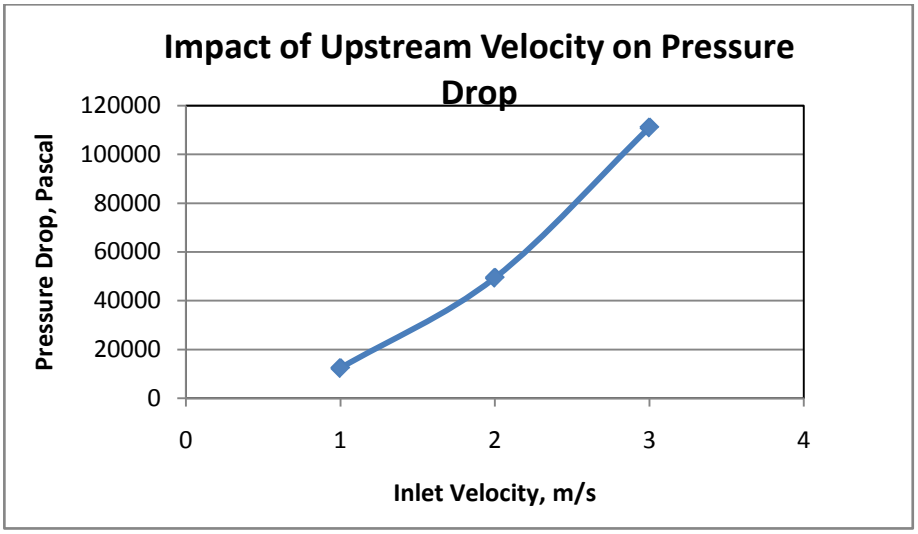


Figure 23: Pressure drop between inlet and outlet of the pipe at different inlet velocity.

It is clear from figure 24 that the total entropy generation obtained by the first method of volumetric entropy generation equation rate was yielding values lower than the second method. The change of upstream velocity from 1 to 3 m/s causes an increase in the total entropy generation from 0.19 to 5.1 W/K according to the pressure drop method.

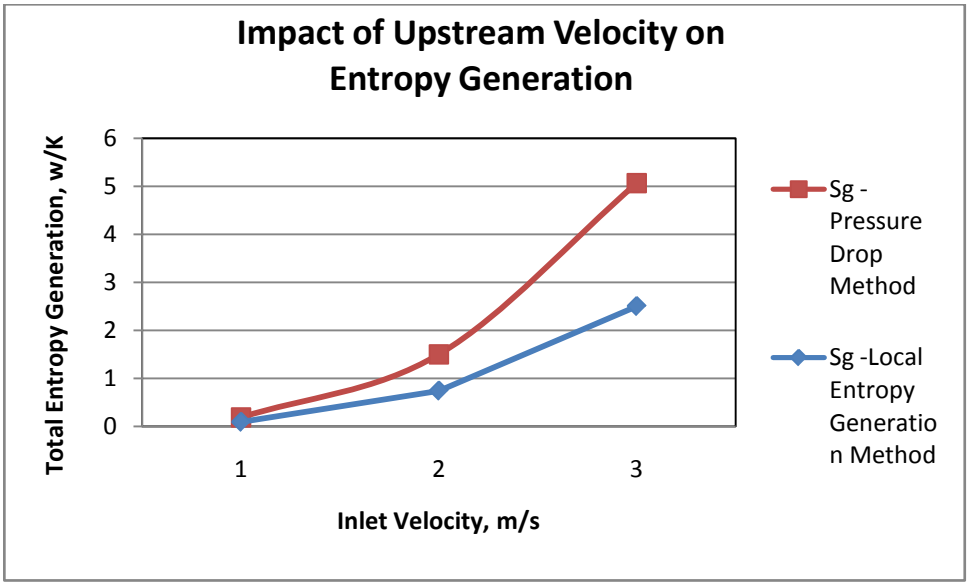


Figure 24: Total entropy generation at different inlet velocity.

From the definition of loss coefficient, it is the ratio of pressure drop to the inlet dynamic pressure. As the inlet dynamic pressure increases the pressure drop increases, this explains that the inlet velocity has no significant effect on the loss coefficient as can be seen from figure 25.

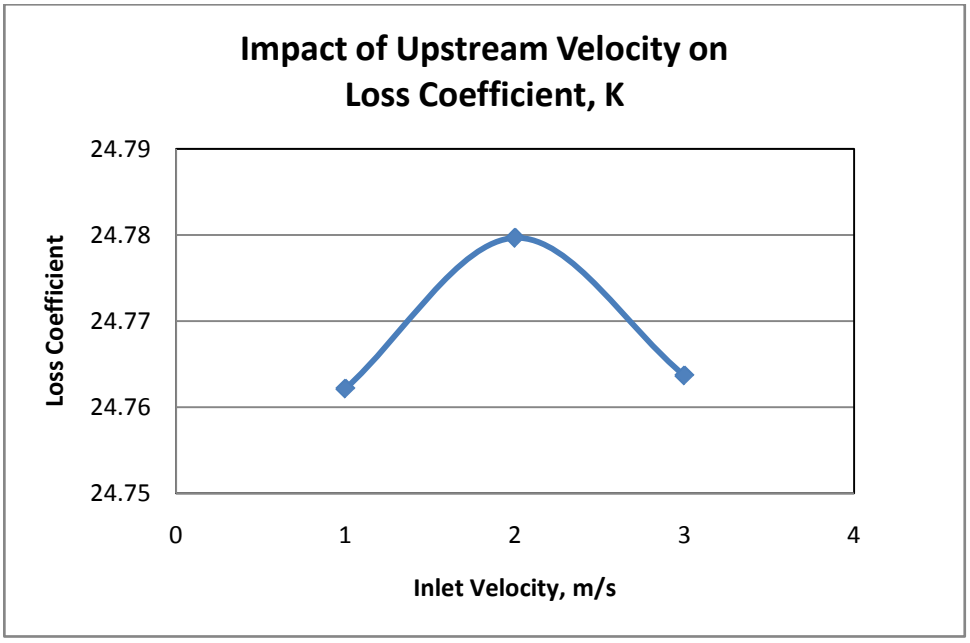


Figure 25: Loss coefficient at different inlet velocity.

The flow coefficient defines the ratio of volumetric flow rate to the square root of pressure drop. It is obvious that the increase of inlet velocity will increase both the flow rate and the pressure drop. From figure 26, it is clear that with increasing the velocity, the flow rate is limited to maximum values to avoid the choking phenomena.

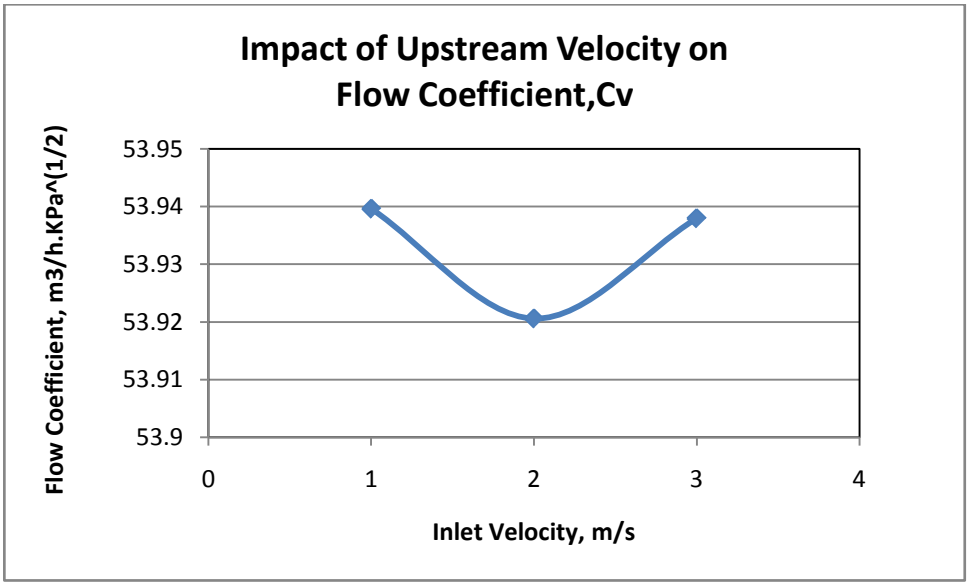


Figure 26: Flow Coefficient at different inlet velocity.

For safe mode of operation, the cavitation index must be less than one in order to avoid cavitation problems. It was found that increasing the upstream velocity increases the cavitation index as shown in figure 27, this due to the fact that as the inlet velocity increases the local pressure drop increases.

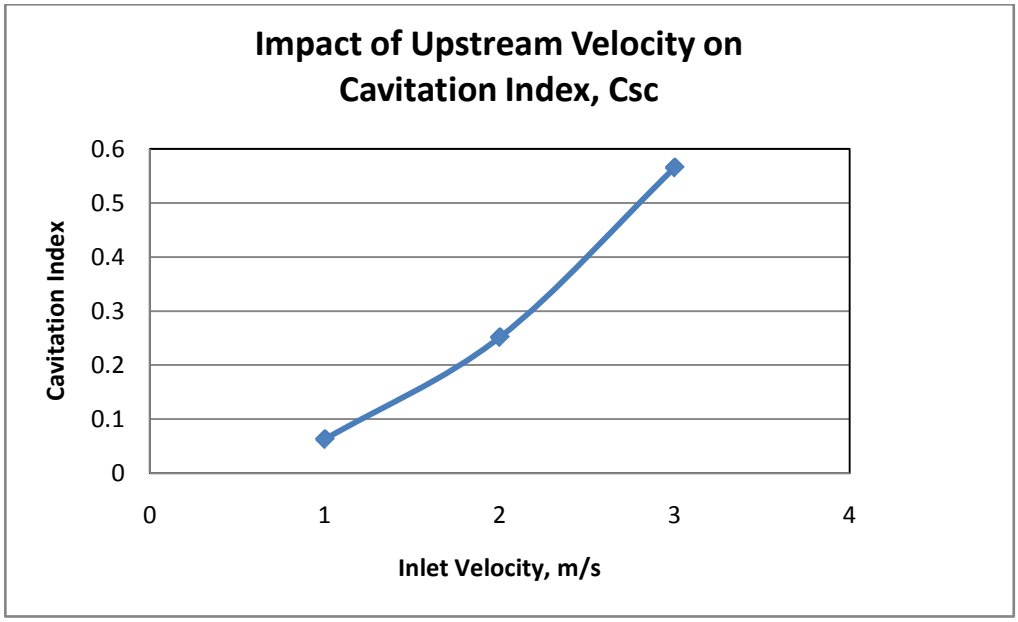


Figure 27: Cavitation Index at different inlet velocity

### 5.2.2 Effect of Upstream Temperature

The effect of temperature in terms of viscosity on the flow characteristics is explored in this section. The change of viscosity was examined by changing the temperature of two fluids; these fluids are water and unused Engine oil. Temperatures of 300, 323, and 353K of water and 293, 300, 313, 323, and 353 of oil were used to conduct this study. The valve position of 45 degree, inlet velocity of 2 m/s, and inlet pressure of 2 A bar were assumed constant as shown in figure 28.

$V_i$ = 2 m/s

$P_i$ = 2 Absolute bar

Water @ $T_i$ = 300, 323, 353 K

Engine Oil @

$T_i$ = 293, 300, 313, 323, 353 K

Throttling valve

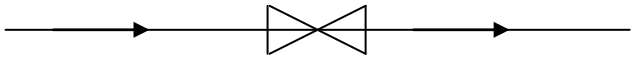

$\theta = 45^{o}$

Figure 28: Upstream conditions and valve position used to study the effect of upstream temperature

From figure 29, it is obvious that the effect of increasing the temperature on the local velocity was not significant in the case of using water as a fluid; however it is more remarkable with the engine oil. This due to the effect of viscosity on irreversibility, as the temperature increases the viscosity decrease and the irreversibility decreases and hence this leads to more kinetic energy. The change of inlet temperature from 300 to 353 K induced an increase in the maximum local velocity from 7.9 to 8.7 m/s in the case of oil and from 8.89 to 8.91 m/s in the case of water. In addition, this confirms the temperature dependant of viscosity in fluids such as oil.

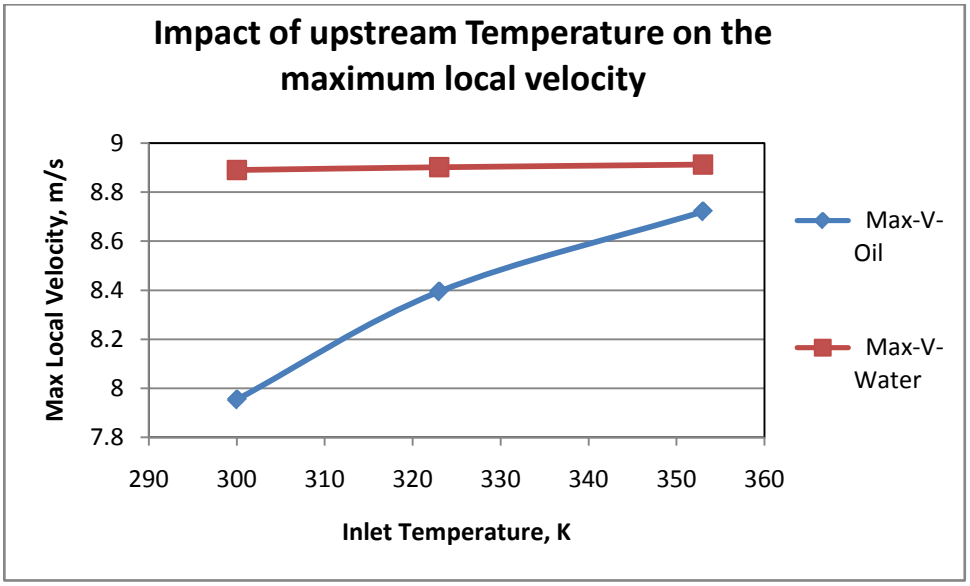


Figure 29: Maximum local velocity at different inlet temperature.

As the temperature increases, the viscosity decreases and this leads to less frictional losses and consequently to less pressure drop as well as less irreversibility. The following figures (30, 31, & 32) show the effect of upstream temperature on the pressure drop and irreversibility in terms of fluid type. The change of inlet temperature from 300 to 353 K decreases the pressure drop from 49.14 to 42.53 KPa in the case of oil and from 49.4 to 48.1 KPa which shows the effect of viscosity on the pressure drop.

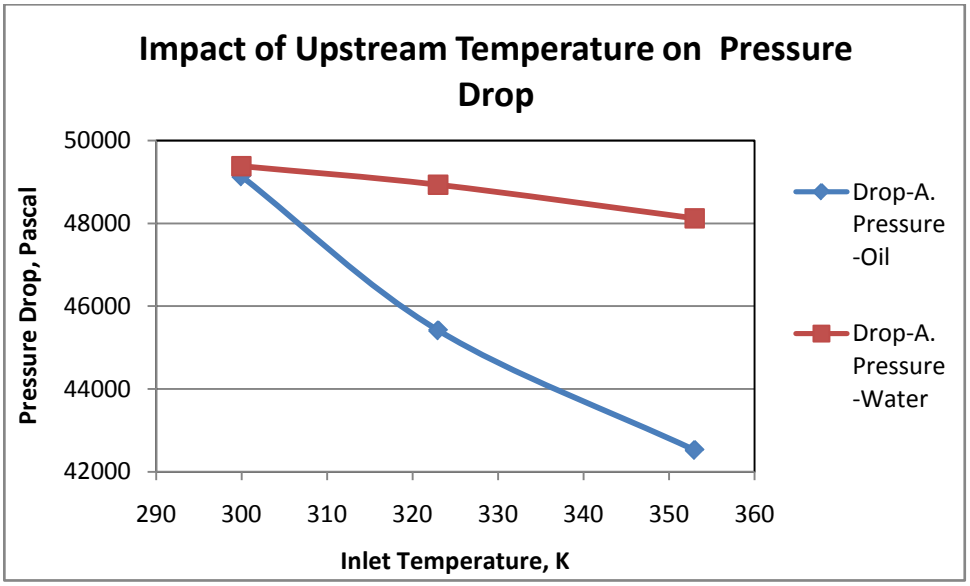


Figure 30: Pressure drop between pipe inlet and outlet at different inlet temperature

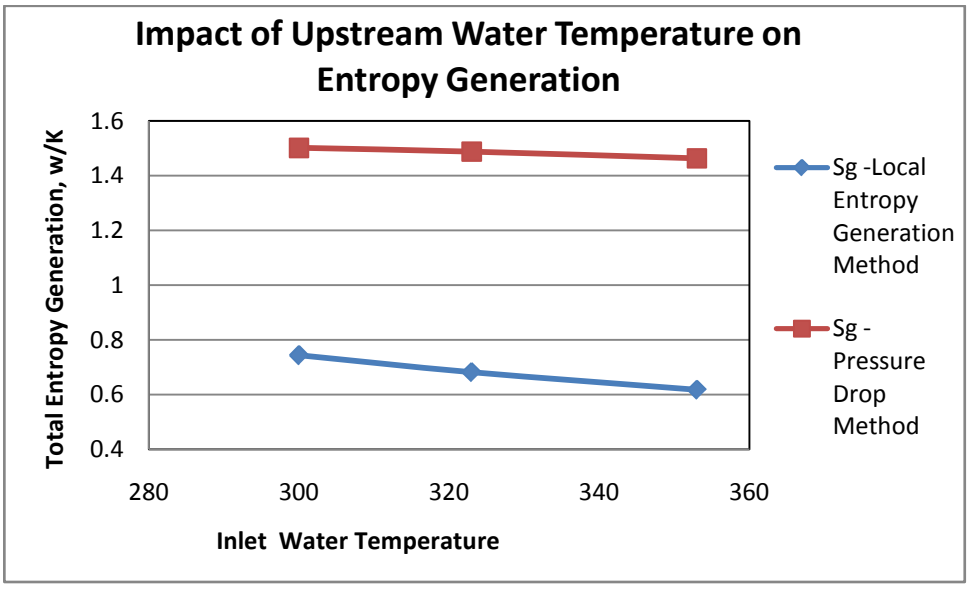


Figure 31: Total entropy generation at different inlet water temperature.

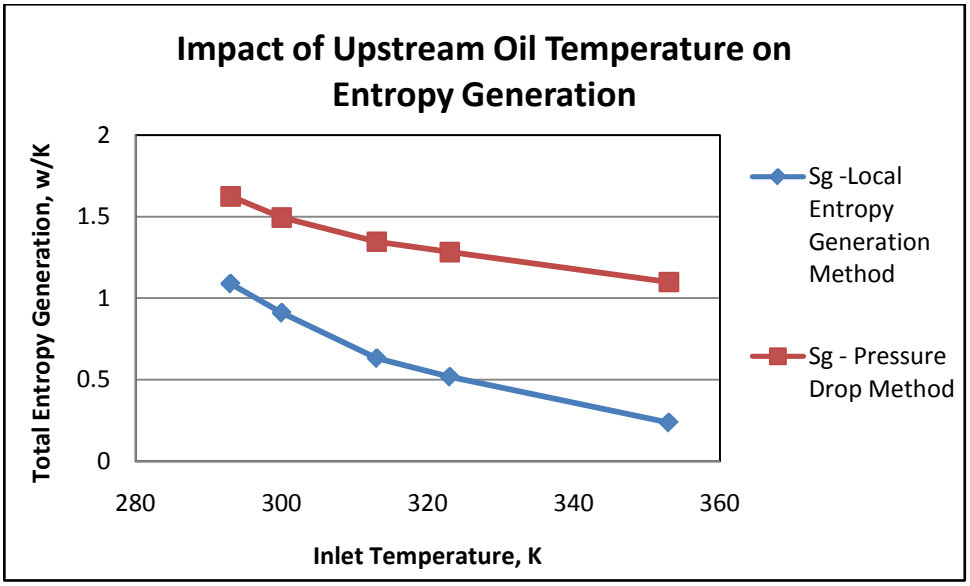


Figure 32: Total entropy generation at different inlet engine oil temperature.

It was found that the change of total entropy generation induced by changing the inlet temperature from 300 to 353 K was 0.038 W/K in case of water while it was around 0.4 W/K in the case of oil according to pressure drop method, see figure 31 and 32.

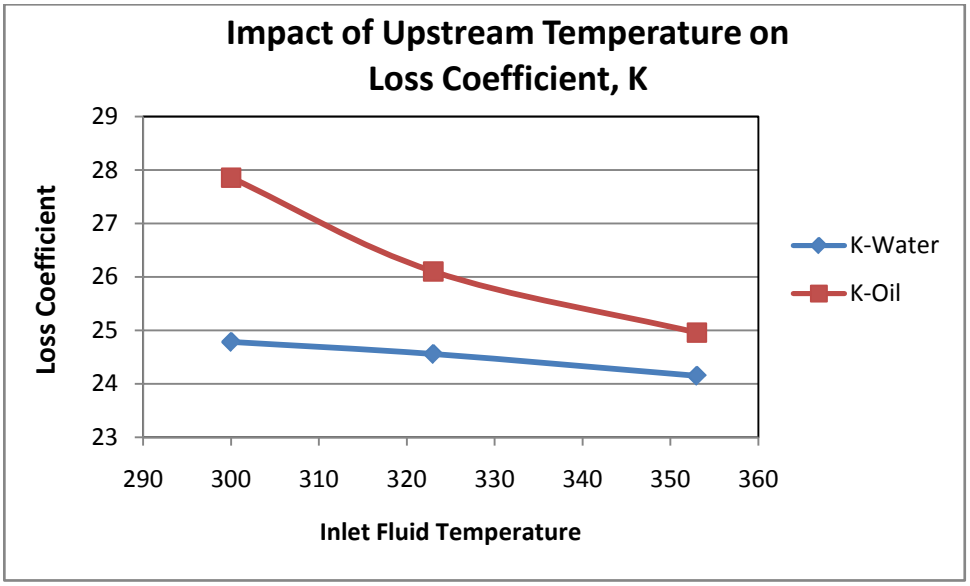


Figure 33: Loss coefficient at different inlet temperature and different fluids.

The viscosity as mentioned previously has its effect on frictional losses and the pressure drop. As the temperature increases the loss coefficient deceases due to the increase of viscosity as shown in the figure 33. The change in the loss coefficient as an effect of changing the temperature from 300 to 353 K was 0.63 in case of water and 2.9 in case of oil.

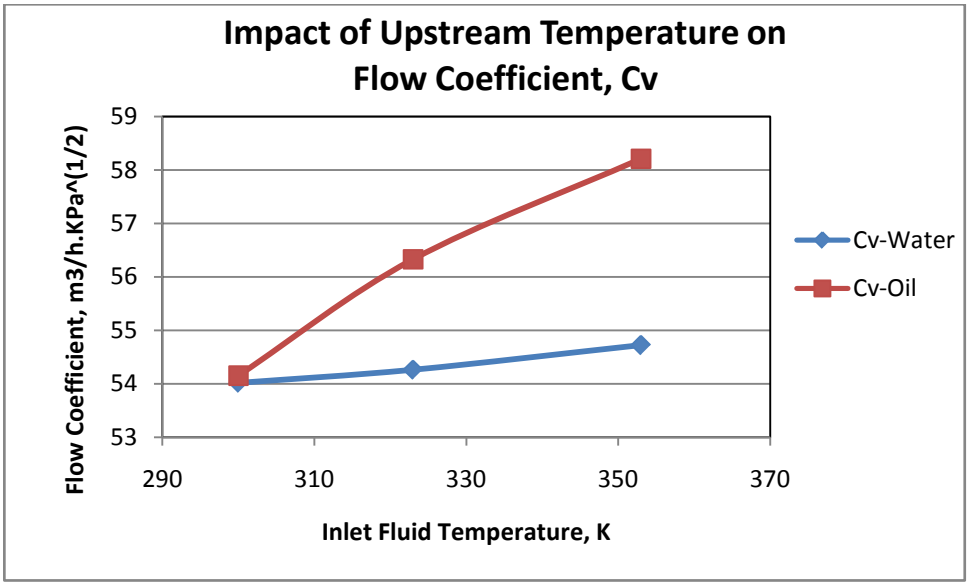


Figure 34: Flow coefficient at different inlet temperature.

As the pressure drop increases the flow rate is limited to a certain maximum value. This can be observed in some operational conditions where as the operator decreases the downstream pressure to get more mass flow rate it remain constant. In this study, it was found that as the inlet temperature increases, the volumetric flow rate increases as shown in figure 34. It was also noticed that the effect of increasing the inlet viscosity in terms of temperature was observed obviously in case of oil. The change of flow coefficient due to the increase of inlet water temperature was 0.7 ($m^3/h.KPa^{1/2}$) while it was 4.06 ($m^3/h.KPa^{1/2}$) in case of oil as a result of changing the temperature from 300 to 353 K.

The cavitation phenomenon in pipe systems is limited by the upstream temperature and pressure as well as the pressure drop. It was found that as the temperature increases the viscosity decreases and the cavitation index decreases as can be seen in figure 35. This is

again related to the pressure drop; as the viscosity increases the pressure drop decreases and consequently the cavitation index deceases. It was also observed that the change of cavitation index values was 0.006 in case of water and 0.034 in case of oil due to the increase of inlet temperature from 300 to 353 K which is considered as a minor change in both cases.

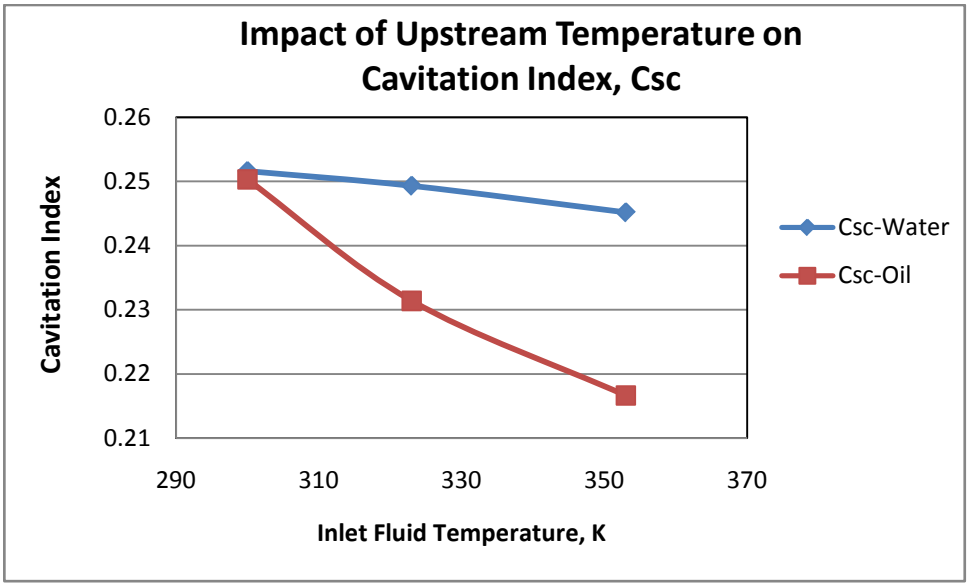


Figure 35: Cavitation Index at different inlet temperature

### 5.2.3 Effect of Valve Position

The position of valve has the major effect on the flow behavior as well as on entropy. As the valve open decreases the drop in pressure increases. In this section, the effect of valve position up to 60 degree on water flow and irreversibility will be examined with two upstream velocities; one at inlet velocity of 1 m/s and the other at 2 m/s. the temperature was set at 300 K and the pressure was set at 2 bar as shown in figure 36.

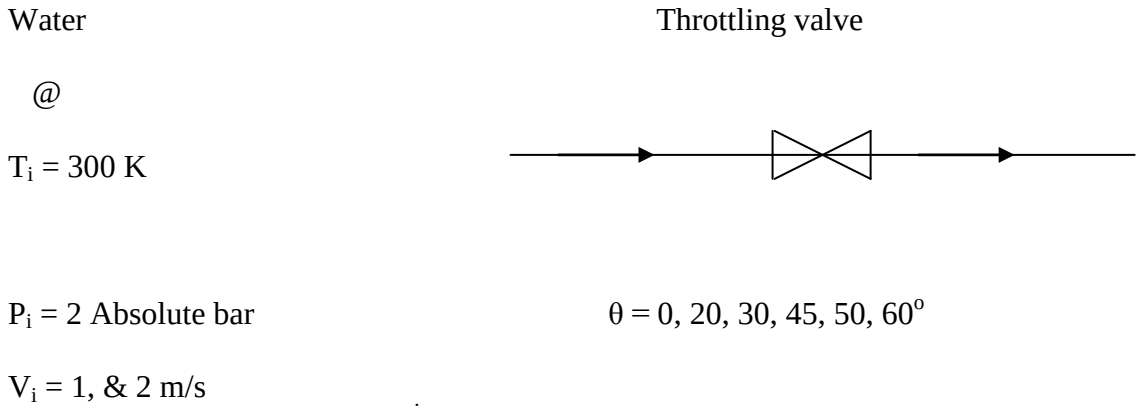


Figure 36: Upstream conditions and valve position used to study the effect of valve position

It was found that the maximum local velocity increases exponentially with the increase of valve angle as shown in figure 37. This shows clearly the effect of throttling process on the flow behavior. The effect of inlet velocity is also obvious on the flow performance; it was found that the increase of maximum local velocity was from 2.2 to 11.62 m/s as a result of increasing the valve angle from 0 to 50 degree in case of upstream velocity of 2 m/s and 1.11 to 5.8 m/s in case of upstream velocity of 2 m/s which almost the double.

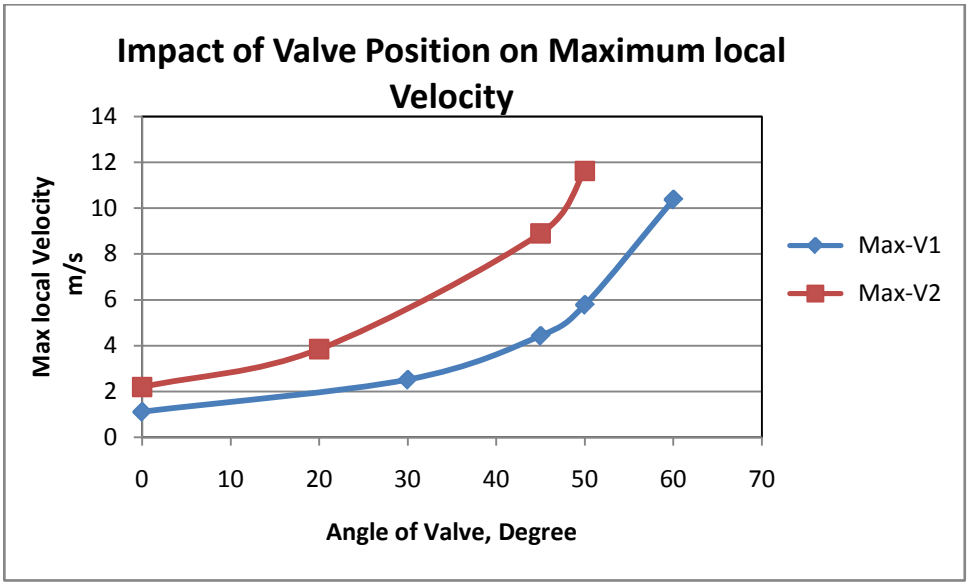


Figure 37: Maximum local velocity at different valve position with different inlet velocity

The effect of valve position on the pressure drop was also examined. It was found that this effect is remarkable with positions of 40 degree and more as shown in figure 38. It can be also observed that with changing the valve angle from 0 to 50 degree the change in pressure drop was from 0.4 to 88.5 KPa at upstream velocity of 2 m/s and was from 0.12 to 22 KPa at upstream velocity of 1 m/s. Therefore doubling the inlet mass flow rate by means of velocity can result in an increase in pressure drop by around four times as can be seen in figure 38.

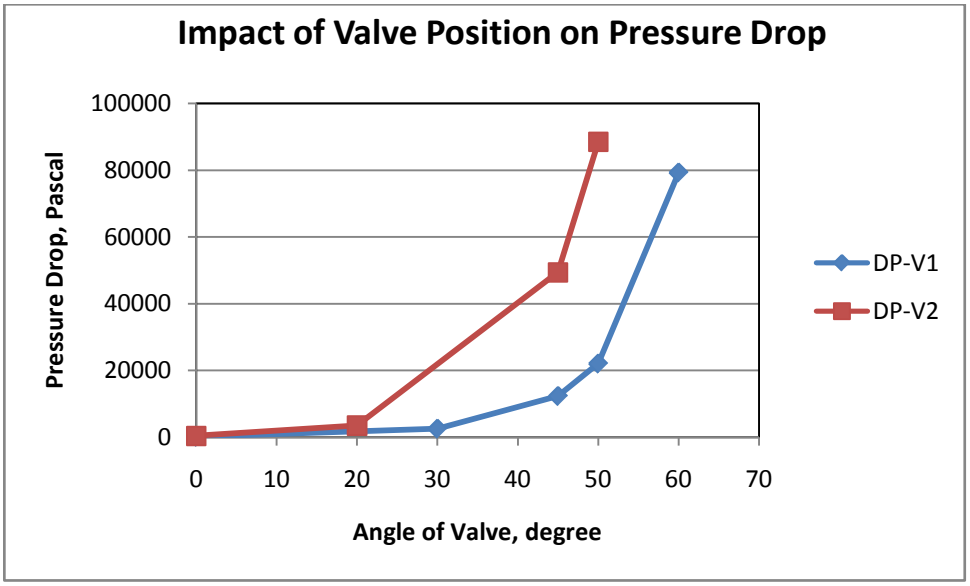


Figure 38: Pressure drop at different valve position with different inlet velocity

The effect of valve position on entropy generation was also examined. It was found that changing the valve position from 0 to 50 degree causes an increase in the entropy generation from 0.0122 to 2.69 W/K at upstream velocity of 2 m/s based on the second method of calculation. Meanwhile, it was also found that the change in entropy generation was from 0.0018 to 1.2 W/K due to the change of valve position from 0 to 60 degree, see figures 39 and 40.

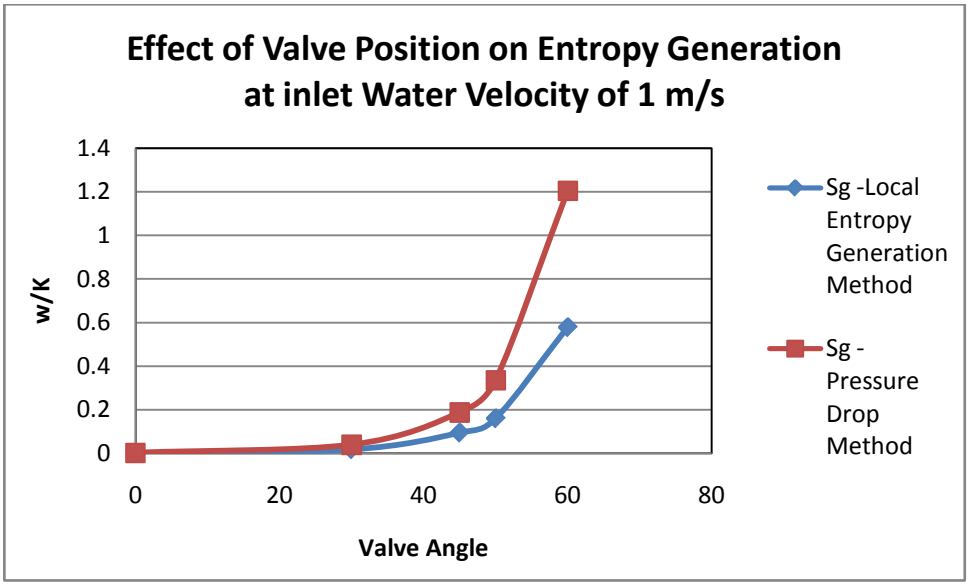


Figure 39: Total entropy generation at different valve position for inlet velocity of 1 m/s

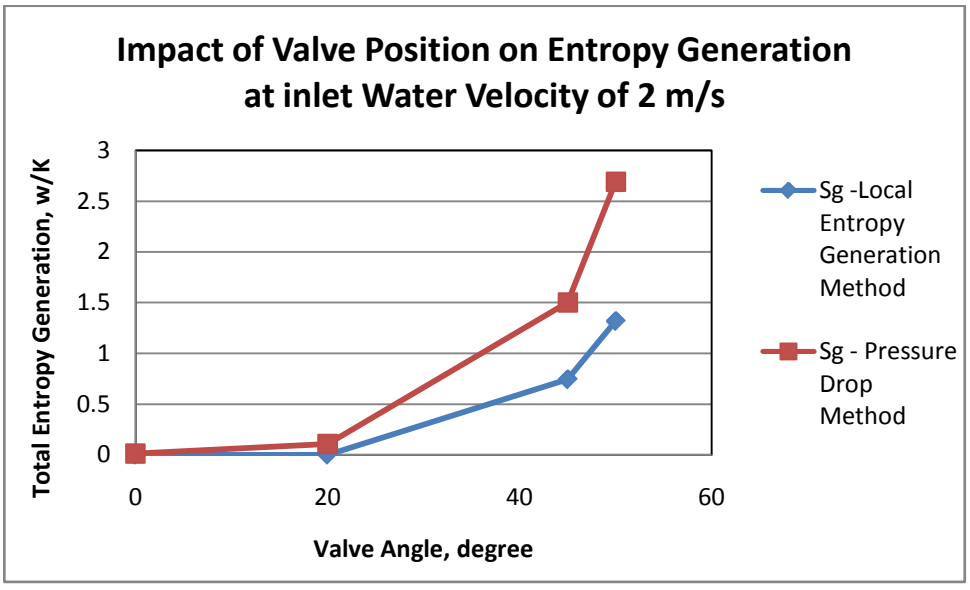


Figure 40: Total entropy generation at different valve position for inlet velocity of 2 m/s.

It was found that the loss coefficient increased exponentially with the decrease of valve open and the increasing of inlet velocity does not have a significant effect on the values of loss coefficient as shown in figure 41. This because of increasing the inlet kinetic energy leads to increasing the drop of pressure and hence a practically constant loss coefficient is obtained. These values are greatly valuable for valve sizing purposes, for different upstream mass flow rates the pressure drop can be estimated as it can be seen later. It was found that the change of valve angle from 0 to 60 degree causes an increase in the loss coefficient from 0.22 to 159.

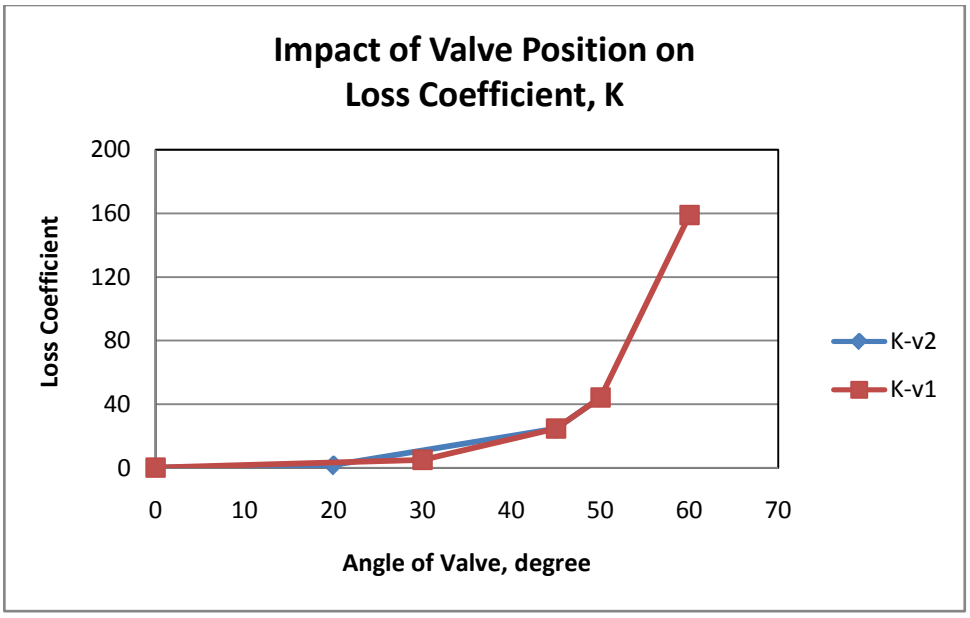


Figure 41: Loss coefficient at different valve position and different inlet velocity.

It can be seen from figure 42 that the decrease of valve open is resulting in a decrease in the flow coefficient due to the increase of pressure drop. The change of valve open from 0 to 60 degree causes a decrease in flow coefficient from an average value of 557 to 21.3. It

also observed that there is not significant effect on the flow coefficient by changing the inlet velocity. Therefore this coefficient can also be used to estimate the pressure drop with different upstream mass flow rate due to the nearly constant flow coefficient values along with different valve positions.

It was found that as the valve open decreases, the pressure drop increases and consequently the cavitation index increases as can be seen from figure 43. It can also be observed that the effect of inlet velocity on the cavitation index was notable, as the inlet flow kinetic energy increases the local maximum velocity increases and as a result low local static pressure areas (Bernoulli Effect). However, all previous cavitation index values are under 1 which shows that these operational conditions are in the safe mode.

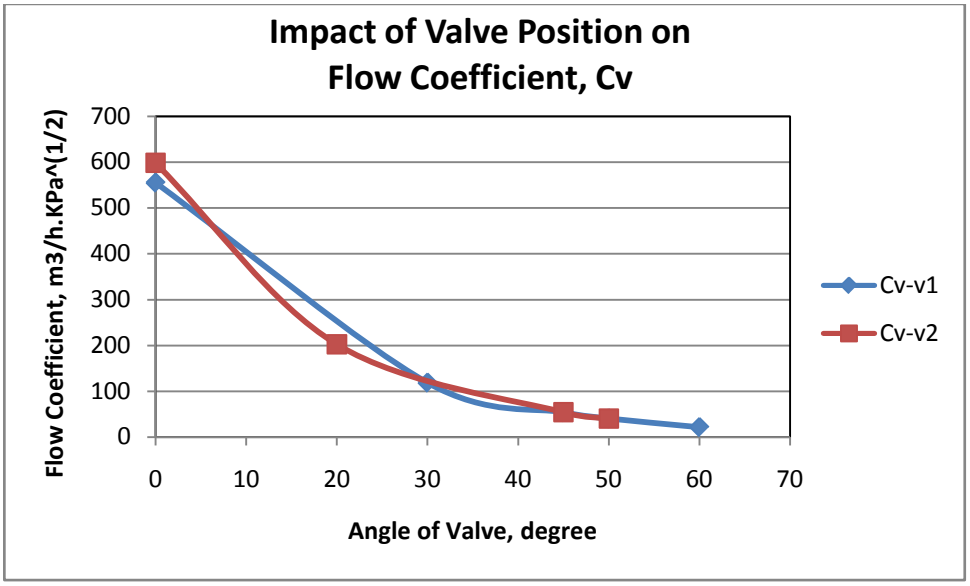


Figure 42: Flow Coefficient at different valve position at different inlet velocity

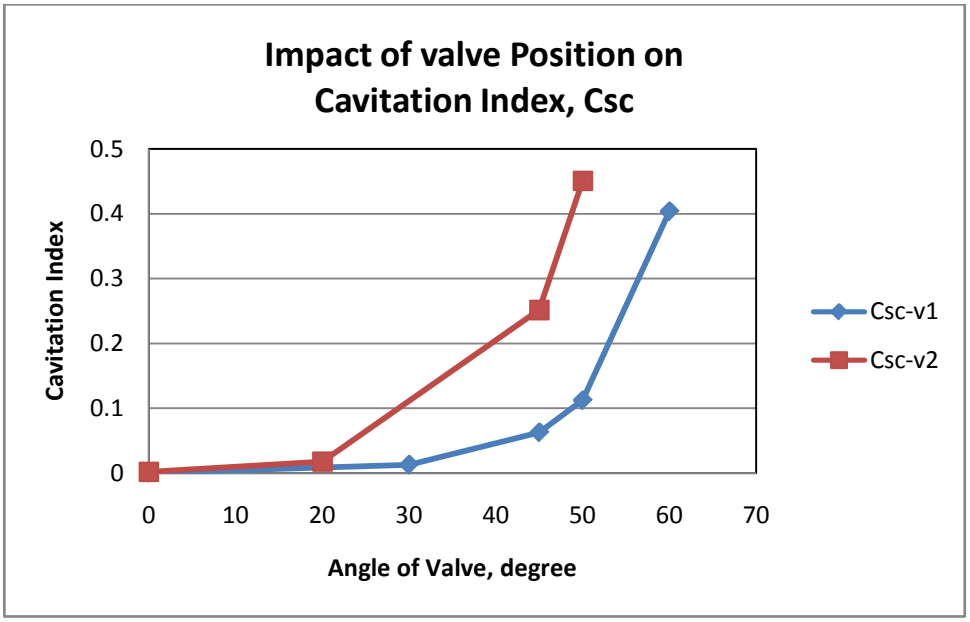


Figure 43: Cavitation Index at different valve position with different inlet velocity

### 5.2.4 Effect of Inlet static Pressure

The drop of pressure across the valve is not affected by the level of upstream static pressure; however it affects the cavitation index. As previously mentioned, the cavitation phenomenon is limited by the upstream velocity, temperature, and pressure drop. The effect of upstream static pressure is explored in this part. The effect of three values of static pressure of 2, 3, ad 4 absolute bar is examined while other conditions remain constant. The upstream temperature of 300 K, upstream velocity of 2 m/s, and valve angle of 45 degree are used as shown in figure 44.

Water

@

$T_i$ = 300 K

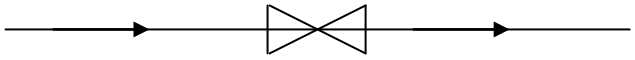

Throttling valve

$P_i$ = 2, 3, & 4 Absolute bar

$V_i$ = 2 m/s

$\theta = 45^o$

Figure 44: Upstream conditions and valve position used to study the effect of upstream pressure

It was noticed that the increase of upstream pressure from 2 to 4 absolute bar resulted in a decrease of 0.25 to 0.12 in the cavitation index as seen from figure 45. It was found that the pressure drop remained constant at around 49.39 kPa with the variation of upstream static pressure. This verifies that the pressure drop is independent of upstream static pressure and shows that the upstream static pressure is an effective parameter in controlling the cavitation index.

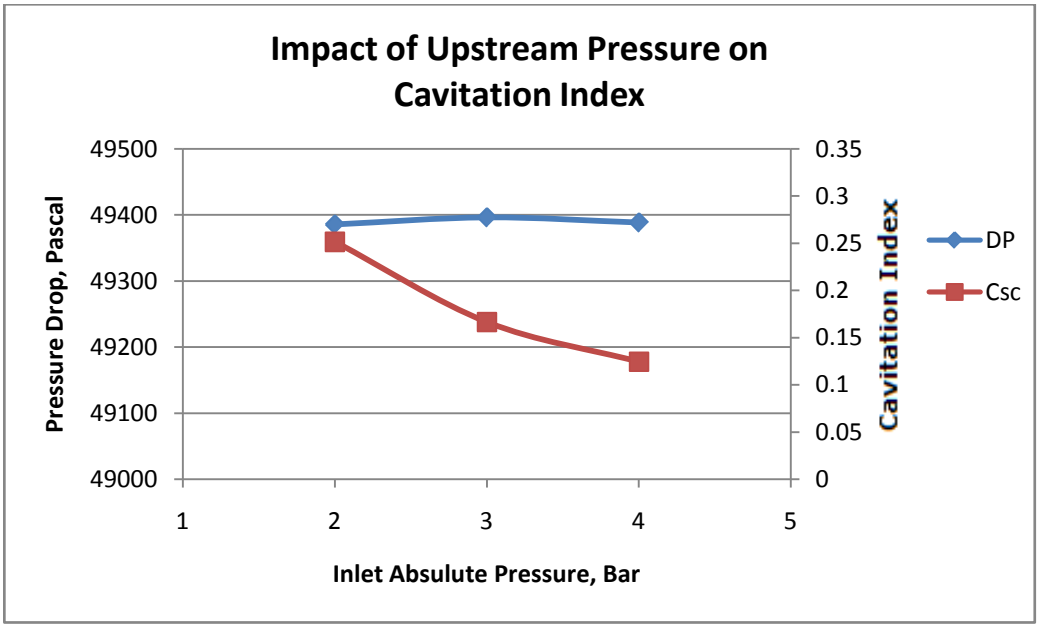


Figure 45: Cavitation Index and pressure drop at different inlet static pressure.

### 5.2.5 Estimation of Other Results

It is clear from previous analysis that the major effects of the examined variables were by the upstream velocity and valve position. Moreover, it was also found that upstream velocity does not have considerable effect on the loss and flow coefficients. Therefore it can be used as effective parameters to estimate the flow performance. In this part the loss coefficient values for different valve positions are used to estimate the pressure drop and cavitation index, refer to figure 41. The variation of operational conditions in this section will be considered as shown in figure 46.

Water @ $T_i$ = 300 K

Throttling valve

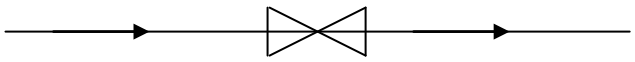

$P_i$ = 2 Absolute bar

$V_i$ = 1, 2, 3, & 4 m/s

$\theta$ = 0, 20, 30, 45, 50, 60$^o$

Figure 46: Upstream conditions and valve position used to study the effect of upstream velocity and valve position

Figures 47 and 48 show the variation of the estimated and predicted pressure drop along with the variation of upstream velocity and valve position. It was found that the pressure drop at upstream velocity of 4 m/s and valve angle of 60 degree was as high as 1270 KPa which is higher than the upstream absolute pressure of 200 KPa which is impossible. The region of single and multi-phase flows were determined by calculating the cavitation index as can be seen in figure 48. This might justify why we have so high pressure drop with the previous operating conditions. It can be seen from figure 48 that the safe operational range of upstream velocity is 1 m/s and less at valve angle of 60 degree. All other safe operational upstream velocity values can be estimated from figure 48 at cavitation index of less than 1. It can also predicted that angles of valve more than 60 degree might cause cavitation problems and limited to an upstream velocity of less than 1 m/s. The total entropy generation was also estimated based on the pressure drop values which show that the loss coefficient can also be used successfully to estimate the entropy generation, see figure 49.

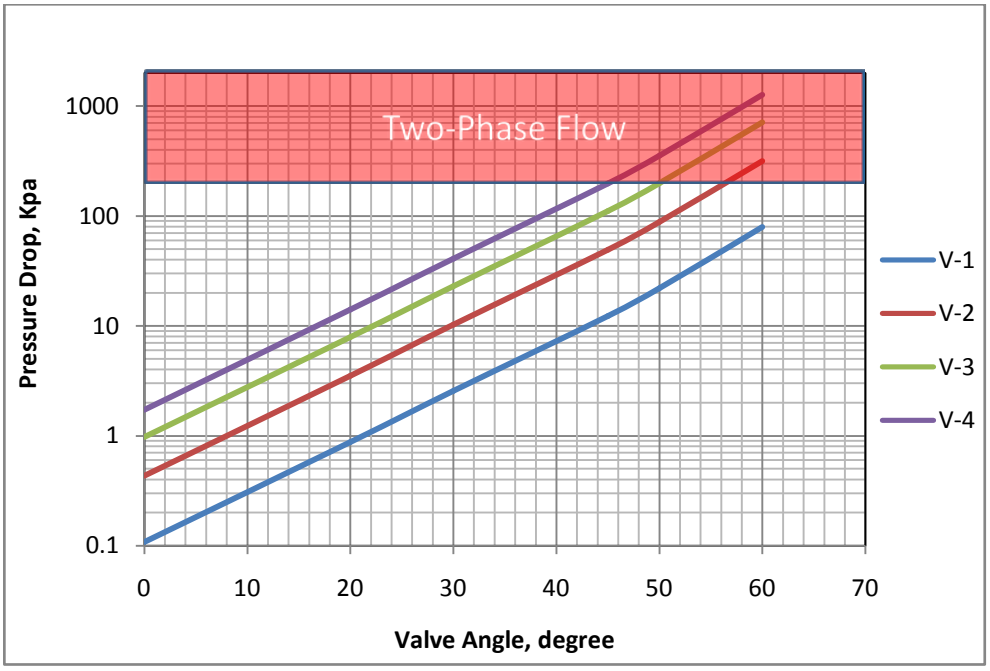


Figure 47: Impact of upstream velocity on the pressure drop at different valve positions

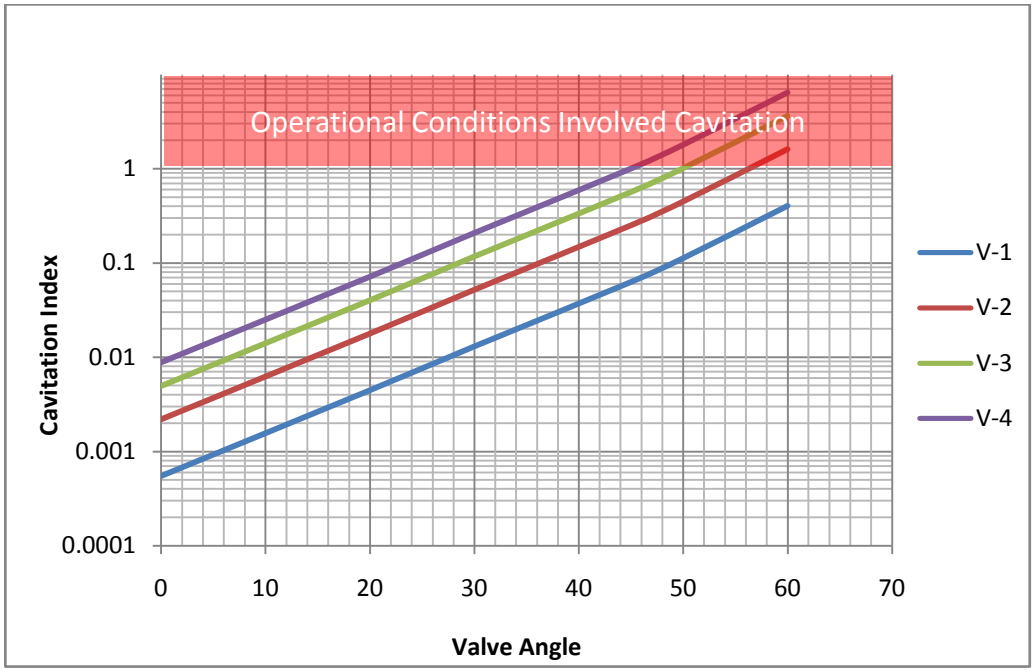


Figure 48: Impact of upstream velocity on the cavitation index at different valve positions

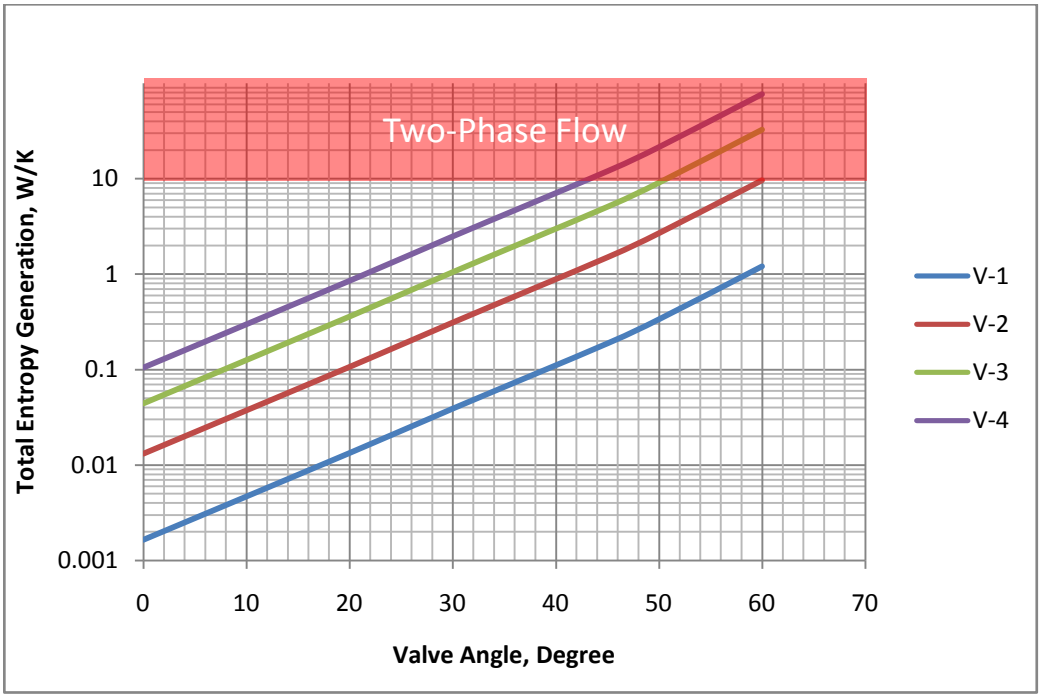


Figure 49: Impact of upstream velocity on entropy generation at different valve positions

### 5.3 Further Investigation on Entropy Generation

It was noticed from previous analysis that the total entropy generation which was calculated by the volumetric entropy generation rate was obtaining lower values than the pressure drop method. This was investigated carefully and it was found that the viscous sublayer should be meshed properly to capture the entire entropy generation rate at thus layer. This can be determined by calculating the dimensionless wall distance ($y^+$).

$$\boldsymbol{y^+ = \frac{\rho . u . y}{\mu}}$$

Where $y^+ \approx 1$ at the viscous sublayer,

**Case study:**

To be able to increase the number of cells at the viscous sublayer and perform it in two dimensional analyses, a simple case from the previous cases for the valve at 0 degree was selected because it can be considered as a pipe, see figure 50.

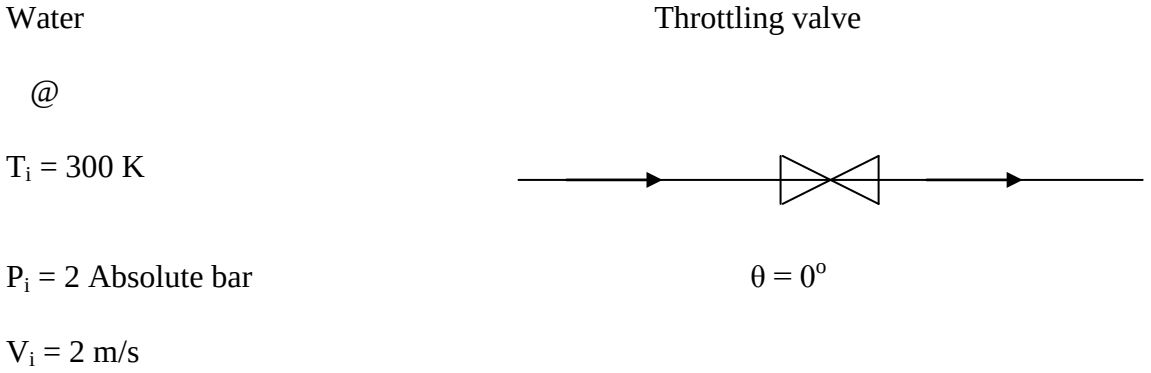


Figure 50: Upstream conditions and valve position used to study the effect of mesh on the total entropy generation

For the above case the predicted total Entropy generation by the *Pressure drop* method was (**0.0122** W/K) while by the *Volumetric Entropy generation rate* method was (**0.000108** W/K). The number of cells at the viscous sublayer was increased in a stepwise manner and the predicted values of the dimensionless wall distance were ranging from 195 to 0.7 as can be seen from table 3. It was noticed that as the $Y^+$ values decreases, the total entropy generation values was approaching the predicted value which was calculated by the pressure drop method, see table 3 and figure 51. It can be concluded that the mesh at the viscous sublayer plays a significant role in determine the viscous entropy generation rate and this method is a mesh dependant.

**Table 3: Variation of total entropy generation with the dimensionless wall distance**

| $Y^+$ | Total Entropy Generation |
|---|---|
| 0.718839 | 0.012155839 |
| 1.437954 | 0.012131332 |
| 6.010865 | 0.011110862 |
| 14.15342 | 0.004942532 |
| 26.32077 | 0.00341975 |
| 53.27755 | 0.00309414 |
| 102.9404 | 0.002099383 |
| 195.3495 | 0.001243737 |

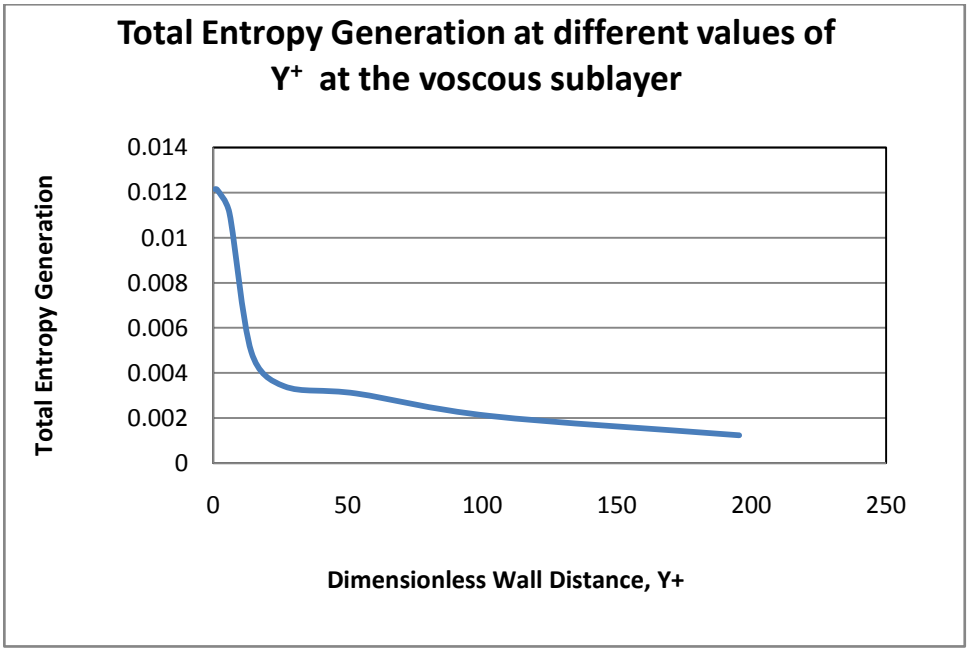


Figure 51: Impact of the mesh dimensionless wall values at the viscous sublayer on the total entropy generation values.

Despite the lower values of the total entropy generation obtained by the volumetric entropy generation rate method, its entropy generation maps might provide us with a useful idea about locations and gradients of irreversibility. In the following, the visual post-processing results are for the engine oil at valve position of 45 degree, inlet temperature of 300 K, inlet pressure of 2 bar, and inlet velocity of 2 m/s.

It was found that the highest entropy generation was at the inlet and outlet of the valve due to the high gradient of velocity as a result of throttling process as clear in figure 52. At the inlet, it was found that the entropy generation is high at the wall of pipe and the edges of the ball as illustrated in figure 52. The effect of velocity gradient on entropy generation at the valve inlet can be demonstrated by referring to figures 53 and 54.

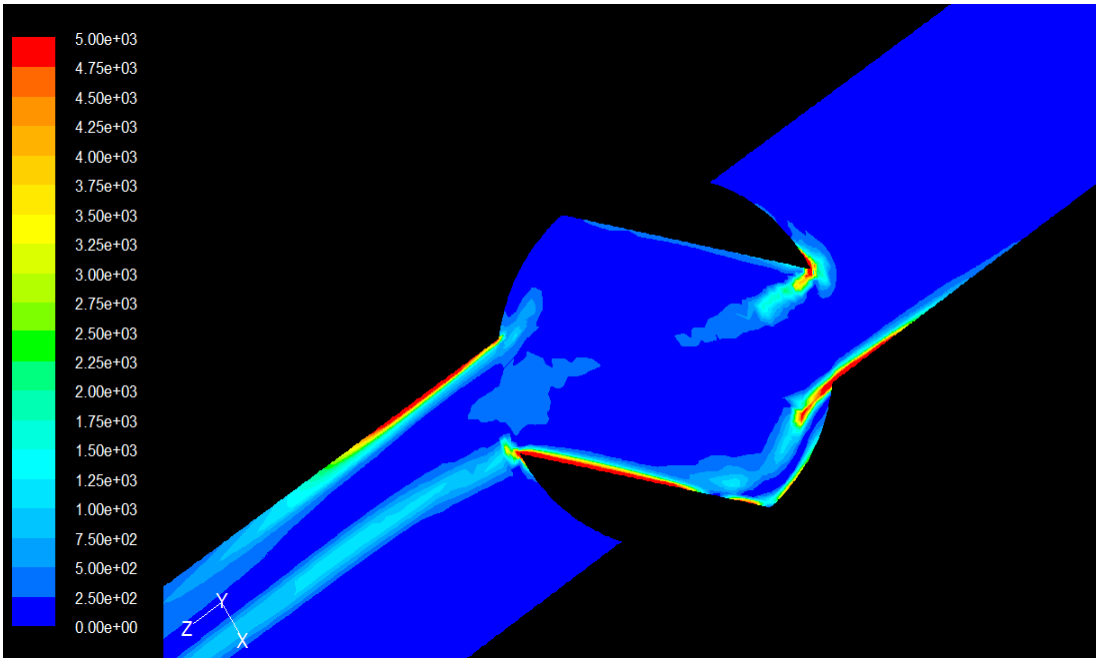


Figure 52: Entropy generation map at X-Z plane

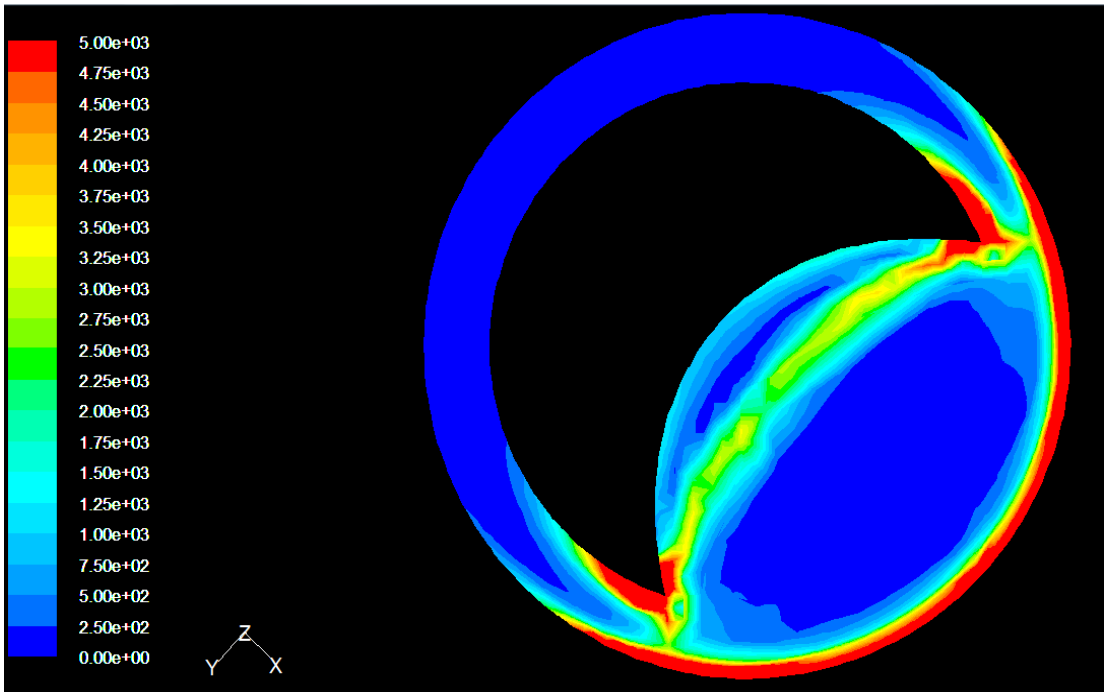


Figure 53: Entropy generation map at X-Y plane at valve inlet.

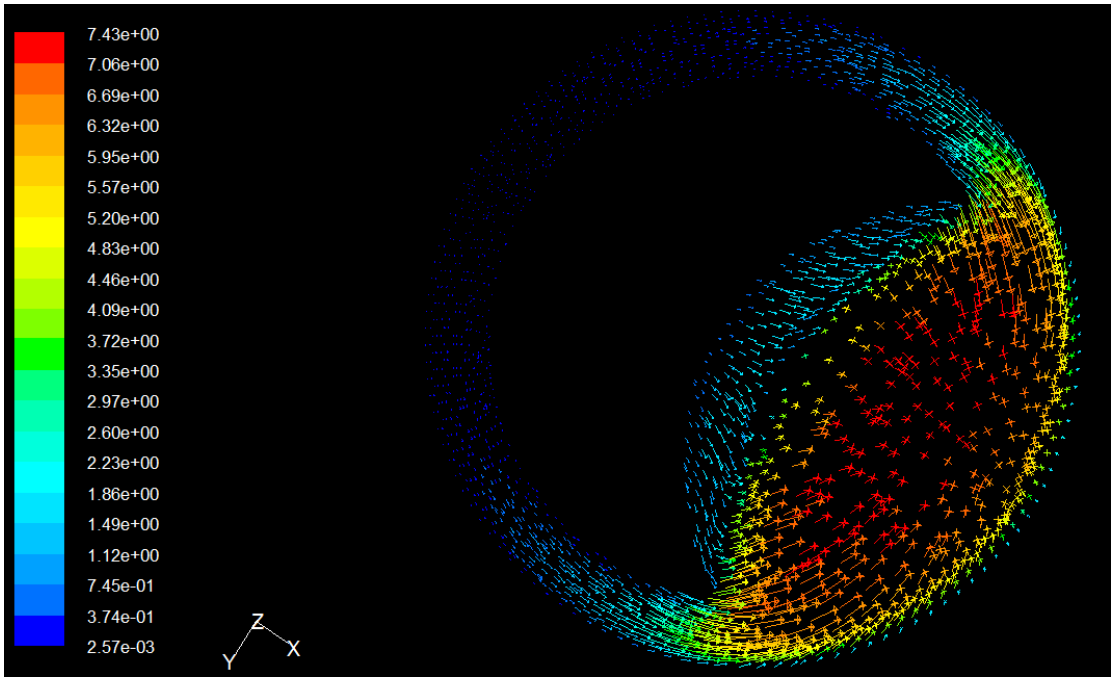


Figure 54: Velocity vectors at X-Y plane at valve inlet.

At 10 and 20 cm after the valve outlet, the entropy map can be comparable as seen in figure 55 and 55. This verifies the effect of axial velocity after the valve outlet on irreversibility.

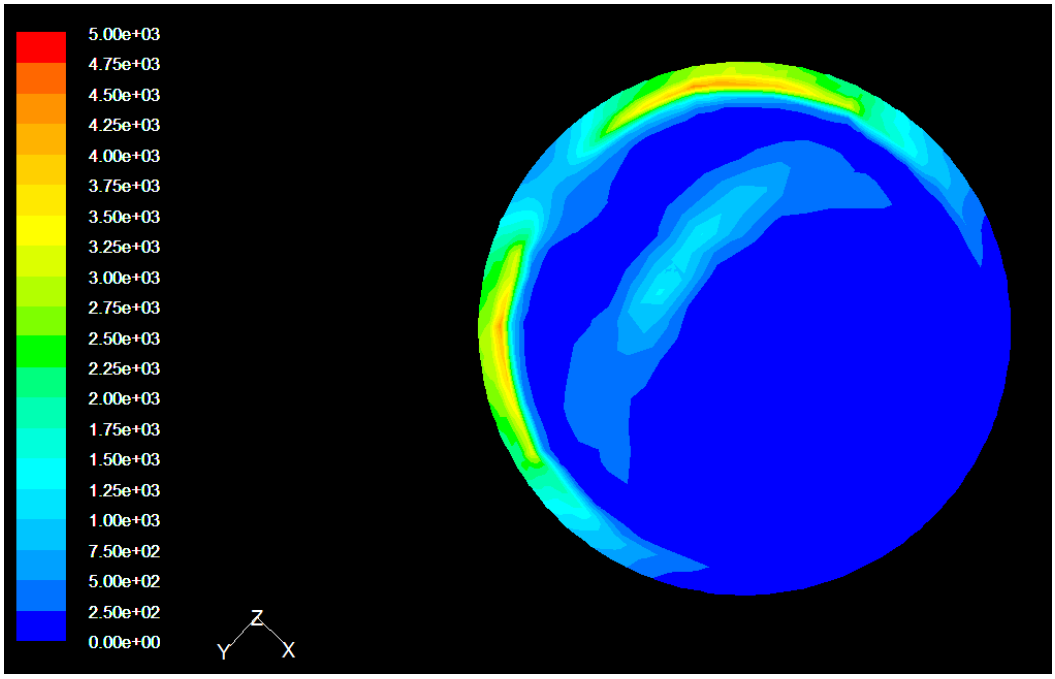


Figure 55: Entropy generation map at 10 cm after the valve outlet at X-Y plane.

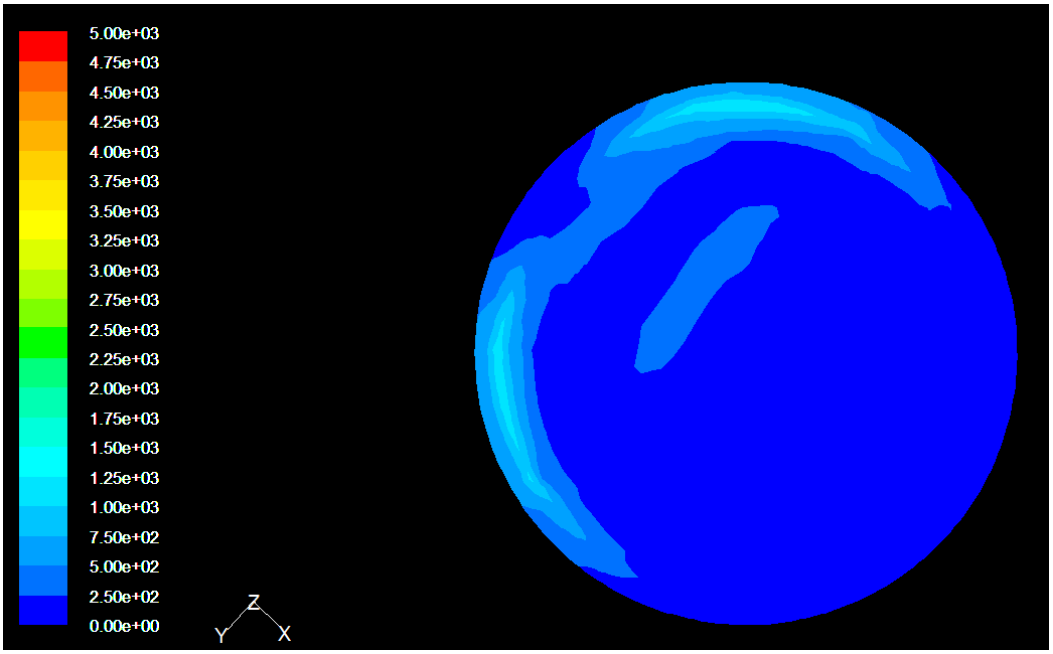


Figure 56: Entropy generation map at 20 cm after the valve outlet at X-Y plane

## 5.4 Validity of the Model

No experimental data were found to be compared with the simulated results obtained in this study. However, the valve at zero position can be considered as a pipe. To find the drop in pressure in pipe theoretically we can use Darcy's equation:

$$H_L = f.\left(\frac{L}{D}\right).\left(\frac{V^2}{2g}\right) \tag{5.4.1}$$

Where $\boldsymbol{H_L}$ is the head loss, $\boldsymbol{f}$ is the friction factor, $\boldsymbol{L}$ is the pipe length, $\boldsymbol{D}$ is the pipe diameter, $\boldsymbol{V}$ is the average fluid velocity, $\boldsymbol{g}$ is the acceleration of gravity.

The friction factor can be found using the Moody diagram in terms of Reynolds number and relative roughness. The tube roughness does not affect the values of friction factor

significantly in turbulent flows therefore a smooth pipe is considered. The upstream conditions for the valve at zero position are as follows; water at temperature of 300 K, velocity of 2 m/s, pressure of 2 bar. The predicted pressure drop by the model is 401 Pascal.

$$\mathrm{Re}_{\mathrm{D_H}} = \frac{\rho V D_H}{\mu}$$

$$\mathrm{Re}_{\mathrm{D_H}} = \frac{996.5 * 2 * 0.0762}{0.00084} = 180{,}794$$

$$f = 0.02$$

$$H_L = 0.02 * \left(\frac{0.75}{0.0762}\right) * \left(\frac{2^2}{2 * 9.81}\right) = 0.041\ m$$

It was found that the calculated head loss using Darcy's equation was 0.041 m which equivalents to 410 Pascal. Meanwhile, the model pressure drop predicted for the same inlet valve operating conditions is 402 Pascal as shown in figure 36. It can thus be concluded that the model predictions are reliable.

# CHAPTER 6

# CONCLUSIONS & RECOMMENDATIONS

## 6.1 Conclusions

The conclusions of the current study are as follows:

1. The flow behaviour and entropy generation rate was investigated in a full port ball valve with a size of three inches.
2. Four turbulent flow models including; Standard $k$-$\varepsilon$ model, Realizable $k$-$\varepsilon$ Model, RNG $k$-$\varepsilon$ Model, and Reynolds Stresses Model were explored to find out the main difference between them as well as to choose the suitable one.
3. It was found that that Standard K-ε, Realizable K-ε, and Reynolds Stresses models are giving more or less the same results while the RNG K-ε model is giving little different profiles and values.
4. Despite the complexity and the high computing time of Reynolds Stresses model it was used to conduct this study as per the recommendations of other authors.
5. Five variables were investigated to explore the effect of upstream conditions as well as the valve position on the flow behavior and irreversibility. These variables

are the viscosity in terms of temperature, inlet velocity, inlet pressure, valve position, and two types of fluids.

6. It was observed that the increase of valve upstream velocity results in the following:
    a. Increasing the upstream velocity from 1 to 3 m/s causes an increase of maximum local velocity from 4 to 13.35 m/s.
    b. An increase in the irreversibility and hence to an increase in the pressure drop.
    c. Does not have a significant effect on the loss coefficient and flow coefficient while its effect was remarkable on the cavitation index.
7. It was found that increasing the valve upstream temperature has an effect on the following:
    a. An inconsequential effect on local maximum velocity in case of water and a slight increase in case of oil due to the viscosity effect.
    b. A decrease in irreversibility and pressure drop due to the decrease in viscosity.
    c. An obvious decrease in the loss coefficient and cavitation index in case of oil and slight in case of water.
8. It was observed that the valve position has the major effect on the flow behaviour and entropy generation. As the valve open decreases the pressure drop and entropy generation increase. It was found that the valve position has the following affects:

a. It has been determined that the maximum local velocity increases exponentially with the increase of valve angle due to the effect of throttling process.
b. It was also found that the effect of valve position and inlet velocity are apparent at valve position of 40 degree and more.
c. It was noticed that the effect of valve position on the loss coefficient and flow coefficient was clear however the effect of inlet velocity with different valve position was insignificant.
d. It was found that the effect of both the valve position and inlet velocity at different valve position was obvious on increasing the cavitation index.

9. It was also noticed that the effect upstream pressure was effective only on the cavitation index. As the inlet pressure increases the cavitation index decreases.
10. The total entropy generation was calculated using the local entropy generation rate and the pressure drop. It was found that the local entropy generation method was giving lower values due to the poor mesh at viscous layer near the wall.
11. It was found that the viscous sublayer should be meshed properly near the wall in order to capture the total entropy generation and this can be determined by calculating the dimensionless wall distance ($y^+$) where its value at the viscous sublayer should be around 1.
12. The entropy maps were presented to give the reader a better understanding about the local entropy generation. It was found that the maximum areas are in the inlet and outlet of the valve due to the throttling process.

13. It was also found that the loss coefficient is an effective parameter to estimate the pressure drop and irreversibility at different valve positions and upstream velocities. Consequently, different pressure drop, cavitation index, and total entropy generation values were estimated in terms of upstream velocity and valve positions.

## 6.2 Recommendations

The Recommendations might be as follows:

1. To investigate the possibility to improve the number of cells near the wall. This can be done with computers with high efficiency.
2. To investigate the flow behaviour through a ball valve with different valve sizes.
3. To investigate the flow behaviour through different types of valve such as globe and gate valves.
4. To investigate using the multi-phase flow models to explore in-depth the cavitation phenomenon in valves.
5. To investigate the performance of valve at transient state and the associated entropy generation.

# Nomenclature

| | |
|---|---|
| $C_{cs}$ | Cavitation index |
| $C_v$ | Flow coefficient |
| $D_H$ | Hydraulic diamter |
| $E$ | Total energy |
| H | Total enthalpy |
| $\widetilde{\mathrm{H}}$ | Mass average enthalpy |
| H | Specific enthalpy |
| I | Turbulence intensity |
| $k$ | Turbulence kinetic energy |
| $K$ | Loss coefficient |
| $k$ | Thermal conductivity |
| $M_t$ | Turbulent Mach number |
| P | Pressure |
| $q$ | Volumetric flow rate |
| $\dot{S}_{gen}$ | Entropy generation rate |
| $S$ | Modulus of the mean rate-of-strain tensor |
| S | Entropy |
| V | velocity |
| $V$ | Axial velocity |
| $v$ | Specific volume |
| T | Temperature |
| T | time |
| $u$ | Velocity component in x-direction |
| $v$ | Velocity component in y-direction |
| $w$ | Velocity component in z-direction |
| $\rho$ | Density |
| U | Internal energy |

| | |
|---|---|
| $\Delta P$ | Pressure drop |
| $\Theta$ | Angle of valve |
| $\lambda$ | The bulk viscosity |
| $\nabla$ | Gradient operator |
| $\mu$ | Dynamic vicosity |
| $\epsilon$ | Rate of dissipation |
| $\mu_t$ | Turbulent or eddy viscosity |
| $\mu_{eff}$ | Effective viscosity |
| $k_{eff}$ | Effective thermal conductivity |
| $\left(\tau_{ij}\right)_{eff}$ | The deviatoric stress tensor |
| $u_{\mathrm{i}}$ | Velocity vector |
| $u^{'}$ | Fluctuation velocity component |
| $\bar{u}$ | Average velocity component |
| $x_j$ | Vectorial directional component |
| $q_j$ | Heat flux vector |
| $\sigma_{ij}$ | Reynolds Stresses tensor |
| $\tau_{ij}$ | Stress tensor |
| $\phi_{ij}$ | The pressure-strain tensor |
| $\phi_{ij,w}$ | The wall-reflection tensor |
| $\epsilon_{ij}$ | The dissipation tensor |
| $\delta_{ij}$ | Kronecker delta |

# REFERENCES

Henderson, A. D., Sargison, J. E., Walker, G. J. and Haynes, J. *"A Numerical Study of the Flow through a Safety Butterfly Valve in a Hydro-Electric Power Scheme"*, 16th Australasian Fluid Mechanics Conference, Australia, 2-7 December, 2007

Adrian Bejan, "Study of Entropy Generation in Fundamental Convective Heat Transfer", Journal of Heat Transfer, 101, 718-725, 1979.

Adrian Bejan, Entropy Generation through Heat and Fluid Flow, New York: John Wiley & Sons, 1982.

Adrian Bejan, "Advanced Engineering Thermodynamics", New York: John Wiley & Sons, 1988.

Adrian Bejan, "Entropy Generation Minimization", NY: CRC Press, 1996.

Ahmet Z. Sahin, "A Second Law Comparison for Optimum Shape of Duct Subjected to Constant Wall Temperature and Laminar Flow", Heat and Mass Transfer, 33, 425-430, 1998(a).

Ahmet Z. Sahin, "A Second Law Analysis of Laminar Viscous Flow through a Duct Subjected to Constant Wall Temperature ", Journal of Heat Transfer, Transactions of the ASME, 120, 76-83, 1998(b).

Ahmet Z. Sahin, Syed M. Zubair, Ahmed Z. Al-Garni, and Ramazan Kahraman, "Effect of Fouling on Operational Cost in Pipe Flow Due to Entropy Generation", Energy Conversion & Management, 41, 1485-1496, 2000.

Ahmet Z. Sahin, "Entropy Generation and Pumping Power in Turbulent Fluid Flow through a Smooth Pipe Subjected to Constant Heat Flux"; Exergy, an International Journal, 2, 314-312, 2002.

Ana Pereira, and Helena M. Ramos, "CFD for hydrodynamic efficiency and design optimization of key elements of SHP", International Journal of Energy and Environment, 1, 6, 937-952, 2010.

Atilla Biyikoglu, "Entropy Generation Due to Flow across the Abrupt Contraction of Pipe Joints", Applied Thermal Engineering, 29, 841–847, 2009.

Iandoli, C.L. and Sciubba, E., 3-D Numerical Calculation of the Local Entropy Generation Rates in a Radial Compressor Stage, Int. J. of Thermodynamics, 8, 2, 83-94, 2005.

Dae-Woong Kim, Sung-Geun Park, Sang-Guk Lee, and Shin-Cheul Kang, "A study on a characteristic of stem friction coefficient for motor operated flexible wedge gate valve", Nuclear Engineering and Design, 239, 1744–1749, 2009.

Makhanlall, D. , Liu, L.H. and Zhang, H.C., "Determination of loss coefficients for high-temperature flow devices: An entropy-based approach", International Journal of Thermal Sciences, 49, 1848-1855, 2010.

F. M. White, "Viscous Fluid Flow", 3rd edition, McGraw-Hill, 2006.

Fluent 6.3 user's manual

Hakan F. Oztop, "Effective Parameters on Second Law Analysis for Semicircular Ducts in Laminar Flow and Constant Wall Heat Flux", International Communications in Heat and Mass Transfer, 32, 266–274, 2005.

Hüseyin Yapıcı, Nesrin Kayataş, Nafiz Kahraman, and Gamze Baştürk, "Numerical Study On Local Entropy Generation In Compressible Flow Through a Suddenly Expanding Pipe", Entropy, 7[1], 38-67, 2005.

Ibanez G., Cuevas S., and Haro M., "Minimization of Entropy Generation by Asymmetric Convective Cooling", International Journal of Heat and Mass Transfer, 46, 1321-1328, 2003.

Ihsan Dagtekin, Hakan F. O ztop, and Ahmet Z. Sahin, "An analysis of entropy generation through a circular duct with different shaped longitudinal fins for laminar flow", International Journal of Heat and Mass Transfer, 48, 171–181, 2005.

Rahaman, M.F., Bari, S. and Veale, D., "Flow Investigation of the Product Fill Valve of Filling Machine for Packaging Liquid Products", Journal of Food Engineering, 85, 252–258, 2008.

Ming-Jyh Chern and Chin-Cheng Wang, "Control of Volumetric Flow-Rate of Ball Valve Using V-Port", Journal of Fluids Engineering, 126, 471–481, 2004.

Ming-Jyh Chern, Chin-Cheng Wang, and Chen-Hsuan Ma, "Performance Test and Flow Visualization of Ball Valve", Experimental Thermal and Fluid Science, 31, 505–512, 2007.

Murat Uygun, Seyhan O., Suat Anci, "Turbulence Modeling for Computational Fluid Dynamics, Part I: Conceptual Outlook", Journal of Aeronautics and Space Technologies, 1, 4 (19-26), 2004.

Nezaket Parlak, Mesut Gur, Vedat Arı, Hasan Kucuk, and Tahsin Engin," Second law analysis of water flow through smooth microtubes under adiabatic conditions", Experimental Thermal and Fluid Science, 35, 60–67, 2011.

Amirante , R., Del Vescovo, G. and Lippolis, A., "Flow forces analysis of an open center hydraulic directional control valve sliding spool ", Energy Conversion and Management, 47, 114–131, 2006.

Raimund Arztmann, "Operation and maintenance of different valve types", Translated and reprinted from conference paper 6. Workshop reciprocating compressors Rheine, Germany, 2002.

Isaev, S. A., Kornev, N.V., Leontiev, A.I. and Hassel, E., "Influence of the Reynolds number and the spherical dimple depth on turbulent heat transfer and hydraulic loss in a narrow channel", International Journal of Heat and Mass Transfer, 53, 178–197, 2010.

Smith Eiamsa-ard, Artit Ridluan, Prachya Somravysin, and Pongjet Promvonge, "Numerical Investigation of Turbulent Flow through a Circular Orifice", KMITL Sci. J., 8,1, 2008.

Smith Eiamsa-ard, "Study on thermal and fluid flow characteristics in turbulent channel flows with multiple twisted tape vortex generators", International Journal of Heat and Mass Transfer, available online, 2010.

Shuang-Ying Wu, Yan Chen, You-Rong Li, and Dan-Ling Zeng, "The Effect of Fouling on Thermodynamic Performance of Forced Convective Heat Transfer through a Duct", Energy Conversion and Management, 48 , 2399–2406, 2007.

Ko, T.H. and Ting, K., "Entropy generation and optimal analysis for laminar forced convection in curved rectangular ducts: A numerical study", International Journal of Thermal Sciences, 45, 138–150, 2006.

Ko, T.H. "Numerical analysis of entropy generation and optimal Reynolds number for developing laminar forced convection in double-sine ducts with various aspect ratios", International Journal of Heat and Mass Transfer, 49, 718-726, 2007.

Fester, V. G., Kazadi, D. M., Mbiya, B. M. and Slatter, P. T., "Loss Coefficients for Flow of Newtonian and Non-Newtonian Fluid through Diaphragm Valves", Chemical Engineering Research and Design, 85 (A9) 1314–1324, 2007.

Fester, V. G., Slatter, P. T., "Dynamic similarity for non-Newtonian fluids in globe valves", chemical engineering research and design, 87, 291–297, 2009.

Versteeg, H.K., Malalasekera, W., "An introduction to computational fluid dynamics, The finite volume method", Longman, Scientific & Technical, Essex, 1995.

Xue Guan Song, Lin Wang, Seok Heum Baek, and Young Chul Park, "Multidisciplinary Optimization of a Butterfly Valve", ISA Transactions, 48, 370-377, 2009.

Yunus A. and Michael B., "Thermodynamics: An Engineering Approach", 2nd edition, McGraw-Hill, 1994.

# VITA

Mr. Holayil A. Al-Otaibi was born in Abha in 1973. He studied all his pre-degree educations in his city, Abha. He joined King Abdulaziz University, Jeddah for Bachelor Degree in Mechanical Engineering and the degree awarded to him in 1998. He joined Saline Water Desalination Research Institute (SWDRI) of Saline Water Conversion Cooperation (SWCC) in 1999 at Al-Jubail as a Mechanical Engineer. Presently, he is holding Senior Mechanical Engineer position in the Institute and involved in several research projects.

He joined KFUPM as a part-time postgraduate student in 2005 for his Master Degree in Mechanical Engineering. During the course of his study, he attended many seminars and conferences and also presented papers relating to his mechanical engineering study.


| | | |
|---|---|---|
| Nationality | : | Saudi |
| Present Address | : | SWCC, P.O.Box 8328, Al-Jubail 31951, Saudi Arabia |
| Permanent address | : | Village - Al-Sharaf, Abha, Saudi Arabia, |
| Mobile number | : | +966 0540607376 |
| Email | : | hlayil@yahoo.com |